DISCRETE AND CONTINUOUS MODELS AND APPLIED COMPUTATIONAL SCIENCE

Volume 31 Number 3 (2023)

Founded in 1993

Founder: PEOPLES' FRIENDSHIP UNIVERSITY OF RUSSIA NAMED AFTER PATRICE LUMUMBA

DOI: 10.22363/2658-4670-2023-31-3

Edition registered by the Federal Service for Supervision of Communications, Information Technology and Mass Media
Registration Certificate: ПИ № ФС 77-76317, 19.07.2019

ISSN 2658-7149 (online); 2658-4670 (print)
4 issues per year.
Language: English.

Publisher: Peoples' Friendship University of Russia named after Patrice Lumumba (RUDN University).
Indexed by Scopus (https://www.scopus.com), Ulrich's Periodicals Directory (http://www.ulrichsweb.com), Directory of Open Access Journals (DOAJ) (https://doaj.org), Russian Index of Science Citation (https://elibrary.ru), CyberLeninka (https://cyberleninka.ru).

Aim and Scope

Discrete and Continuous Models and Applied Computational Science arose in 2019 as a continuation of RUDN Journal of Mathematics, Information Sciences and Physics. RUDN Journal of Mathematics, Information Sciences and Physics arose in 2006 as a merger and continuation of the series "Physics", "Mathematics", "Applied Mathematics and Computer Science", "Applied Mathematics and Computer Mathematics".

Discussed issues affecting modern problems of physics, mathematics, queuing theory, the Teletraffic theory, computer science, software and databases development.

It's an international journal regarding both the editorial board and contributing authors as well as research and topics of publications. Its authors are leading researchers possessing PhD and PhDr degrees, and PhD and MA students from Russia and abroad. Articles are indexed in the Russian and foreign databases. Each paper is reviewed by at least two reviewers, the composition of which includes PhDs, are well known in their circles. Author's part of the magazine includes both young scientists, graduate students and talented students, who publish their works, and famous giants of world science.

The Journal is published in accordance with the policies of COPE (Committee on Publication Ethics). The editors are open to thematic issue initiatives with guest editors. Further information regarding notes for contributors, subscription, and back volumes is available at http://journals.rudn.ru/miph.

E-mail: miphj@rudn.ru, dcm@sci.pfu.edu.ru.

EDITORIAL BOARD

Computer Design: *Anna V. Korolkova*, *Dmitry S. Kulyabov*
English text editors: *Nikolay E. Nikolaev*, *Ivan S. Zaryadov*, *Konstantin P. Lovetskiy*

Address of editorial board:
Ordzhonikidze St., 3, Moscow, Russia, 115419
Tel. +7 (495) 955-07-16, e-mail: publishing@rudn.ru
Editorial office:
Tel. +7 (495) 952-02-50, miphj@rudn.ru, dcm@sci.pfu.edu.ru
site: http://journals.rudn.ru/miph

Paper size 70×100/16. Offset paper. Offset printing. Typeface "Computer Modern".
Conventional printed sheet 10.13. Printing run 500 copies. Open price. The order 1119.
PEOPLES' FRIENDSHIP UNIVERSITY OF RUSSIA NAMED AFTER PATRICE LUMUMBA
6 Miklukho-Maklaya St., 117198 Moscow, Russian Federaion
Printed at RUDN Publishing House:
3 Ordzhonikidze St., 115419 Moscow, Russia,
Ph. +7 (495) 952-04-41; e-mail: publishing@rudn.ru

Discrete & Continuous Models
& Applied Computational Science
ISSN 2658-7149 (online), 2658-4670 (print)
2023, 31 (3) 204
http://journals.rudn.ru/miph

Contents

Discrete & Continuous Models
& Applied Computational Science
ISSN 2658-7149 (online), 2658-4670 (print)

2023, 31 (3) 205–217
http://journals.rudn.ru/miph

Research article

UDC 519.872
DOI: 10.22363/2658-4670-2023-31-3-205-217
EDN: LACMZU

Asymptotic diffusion analysis of the retrial queuing system with feedback and batch Poisson arrival

Anatoly A. Nazarov[1],
Svetlana V. Rozhkova[1, 2], **Ekaterina Yu. Titarenko**[2]

[1] *Institute of Applied Mathematics and Computer Science,*
National Research Tomsk State University,
36 Lenin Avenue, Tomsk, 634050, Russian Federation
[2] *School of Core Engineering Education,*
National Research Tomsk Polytechnic University,
30 Lenin Avenue, Tomsk, 634050, Russian Federation

(received: May 18, 2023; revised: July 25, 2023; accepted: September 8, 2023)

Abstract. The mathematical model of the retrial queuing system $M^{[n]}/M/1$ with feedback and batch Poisson arrival is constructed. Customers arrive in groups. If the server is free, one of the arriving customers starts his service, the rest join the orbit. The retrial and service times are exponentially distributed. The customer whose service is completed leaves the system, or reservice, or goes to the orbit. The method of asymptotic diffusion analysis is proposed for finding the probability distribution of the number of customers in orbit. The asymptotic condition is growing average waiting time in orbit. The accuracy of the diffusion approximation is obtained.

Key words and phrases: retrial queuing system, batch arrival, feedback, asymptotic diffusion analysis

1. Introduction

There are situations in practice where an arriving customer that sees the server being occupied temporarily leaves the system or goes to orbit. In some random time customer retries to occupy a server again. These situations are modeled as retrial queuing systems. In addition, there are queuing systems in which a customer that has already received service requires a second service. It depends on the quality of the received service or external factors. Classical examples are communication networks in which erroneously transmitted data is retransmitted. The functioning of such systems is described by retrial queuing systems with feedback.

There are many reviews on the study of queuing systems with repeated calls, for example [1, 2]. Models with feedback, instantaneous and delayed, have also been intensively studied in the last two decades [3–5]. At the same

time, classical methods do not allow us to evaluate the characteristics of such systems. The application of asymptotic analysis methods makes it possible to obtain the asymptotic characteristics of the system under various limiting conditions. For example, in [6], a stationary probability distribution of the number of customers in orbit was obtained under conditions of a large delay of customers in orbit. To perform more detailed and accurate analysis of the model a method of asymptotic diffusion analysis is applied [7].

In this paper, we study retrial queuing systems with single server, batch Poisson arrival process, instantaneous and delayed feedback. The retrial and service times are exponentially distributed. A diffusion approximation of the probability distribution of the number of customers in orbit is constructed. It is shown that the accuracy of the diffusion approximation is higher then the accuracy of Gaussian approximation obtained in [6].

2. System description

We consider the queuing system $M^{[n]}/M/1$ with repeated calls (see figure 1) with Poisson batch input flow with a parameter λ and given probabilities q_ν of occurrence of ν customers in the group $\left(\nu > 0,\, q_0 = 0, \sum_{\nu=1}^{\infty} q_\nu = 1\right)$. If the server is free, then one customer receive service, the rest of customers go to the orbit. If the server is busy, the arriving customers join the orbit. The service time is exponentially distributed with parameter μ. A customer whose service is completed leaves the system with probability r_0, receives service again with probability r_1 or goes to the orbit with probability r_2, thus $r_0 + r_1 + r_2 = 1$. In orbit, customers wait for a time distributed exponentially with parameter σ, after which they repeat an attempt to occupy the server. In case of an unsuccessful attempt, the customers remain in orbit.

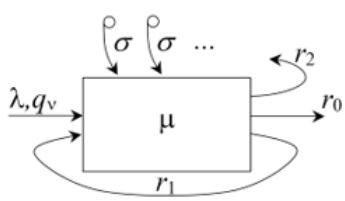

Figure 1. Queuing system model with retrial calls and feedback

We denote by $i(t)$ the number of customers in orbit at time t, the process $n(t)$ determines the state of the server as follows:

$$n(t) = \begin{cases} 0, & \text{if the server is idle;} \\ 1, & \text{if the server is busy.} \end{cases}$$

The two-dimensional process $\{i(t), n(t)\}$ is a continuous-time Markov chain. It is required to find the probability distribution of the number of customers in orbit, taking into account the state of the server

$$P_n(i,t) = P\{n(t) = n,\ i(t) = i\}, \quad n = 0, 1; \quad i = \overline{0, \infty}.$$

We compose a system of Kolmogorov differential equations for the probability distribution $P_n(i,t)$

$$\begin{cases} \dfrac{\partial P_0(i,t)}{\partial t} = -(\lambda + i\sigma)P_0(i,t) + \mu r_0 P_1(i,t) + \mu r_2 P_1(i-1,t); \\ \dfrac{\partial P_1(i,t)}{\partial t} = (i+1)\sigma P_0(i+1,t) + (\mu r_1 - \mu - \lambda)P_1(i,t) + \\ \qquad + \displaystyle\sum_{\nu=1}^{i+1} \lambda q_\nu P_0(i-\nu+1,t) + \sum_{\nu=1}^{i} \lambda q_\nu P_1(i-\nu,t). \end{cases} \tag{1}$$

We consider the partial characteristic functions of the number of customers in the orbit $H_n(u,t) = \sum\limits_{i=0}^{\infty} e^{jui} P_n(i,t)$ and the characteristic function for the number of customers in the batch $h(u) = \sum\limits_{\nu=1}^{\infty} e^{ju\nu} q_\nu$, where $j = \sqrt{-1}$. Then we take into account that

$$\frac{\partial H_n(u,t)}{\partial u} = \sum_{i=0}^{\infty} ij e^{jui} P_n(i,t),$$

$$\sum_{i=0}^{\infty}\sum_{\nu=1}^{i} q_\nu e^{jui} P_1(i-\nu,t) = h(u)H_1(u,t),$$

$$\sum_{i=0}^{\infty}\sum_{\nu=1}^{i+1} q_\nu e^{jui} P_0(i-\nu+1,t) = e^{-ju}h(u)H_0(u,t),$$

and rewrite system (1) as

$$\begin{cases} \dfrac{\partial H_0(u,t)}{\partial t} = \sigma j \dfrac{\partial H_0(u,t)}{\partial u} - \lambda H_0(u,t) + \left(\mu r_0 + \mu r_2 e^{ju}\right) H_1(u,t); \\ \dfrac{\partial H_1(u,t)}{\partial t} = -\sigma j e^{-ju} \dfrac{\partial H_0(u,t)}{\partial u} + \lambda e^{-ju} h(u) H_0(u,t) + \\ \qquad + \left(\lambda h(u) - \mu r_0 - \mu r_2 - \lambda\right) H_1(u,t). \end{cases} \tag{2}$$

The total characteristic function $H(u,t)$ of the number of customers in orbit is $H(u,t) = H_0(u,t) + H_1(u,t)$. We summarize the equations of system (2) and write

$$\frac{\partial H(u,t)}{\partial t} = \sigma j \left(1 - e^{-ju}\right) \frac{\partial H_0(u,t)}{\partial u} + \lambda \left(e^{-ju} h(u) - 1\right) H_0(u,t) + \\ + \left(\mu r_2 \left(e^{ju} - 1\right) + \lambda \left(h(u) - 1\right)\right) H_1(u,t). \tag{3}$$

3. The first stage of asymptotic. A transfer coefficient

We solve the equations for the characteristic function (2) under the asymptotic condition of the growing average waiting time in orbit, that is, we

assume that $\sigma \to 0$. We denote $\sigma = \varepsilon$ and make the following substitutions in system (2)

$$\tau = \varepsilon t, \quad u = \varepsilon w, \quad H_n(u,t) = F_n(w,\tau,\varepsilon), \quad n = 0,1,$$

$$\frac{\partial H_0(u,t)}{\partial u} = \frac{1}{\varepsilon}\frac{\partial F_0(w,\tau,\varepsilon)}{\partial w}, \quad \frac{\partial H_n(u,t)}{\partial t} = \varepsilon\frac{\partial F_n(w,\tau,\varepsilon)}{\partial \tau}, \quad n = 0,1,$$

then we get a system of equations

$$\begin{cases} \varepsilon\dfrac{\partial F_0(w,\tau,\varepsilon)}{\partial \tau} = j\dfrac{\partial F_0(w,\tau,\varepsilon)}{\partial w} - \lambda F_0(w,\tau,\varepsilon) + \\ \qquad + \left(\mu r_0 + \mu r_2 e^{jw\varepsilon}\right) F_1(w,\tau,\varepsilon); \\ \varepsilon\dfrac{\partial F_1(w,\tau,\varepsilon)}{\partial \tau} = -je^{-jw\varepsilon}\dfrac{\partial F_0(w,\tau,\varepsilon)}{\partial w} + \lambda e^{-jw\varepsilon}h(w,\varepsilon)F_0(w,\tau,\varepsilon) + \\ \qquad + \left(\lambda h(w,\varepsilon) - \mu r_0 - \mu r_2 - \lambda\right) F_1(w,\tau,\varepsilon). \end{cases} \tag{4}$$

We look for a solution to the equations in the form $F_n(w,\tau,\varepsilon) = R_n e^{jwx(\tau)}$, then

$$\begin{cases} \varepsilon jwx'(\tau)R_0 = -x(\tau)R_0 - \lambda R_0 + \left(\mu r_0 + \mu r_2 e^{jw\varepsilon}\right) R_1; \\ \varepsilon jwx'(\tau)R_1 = e^{-jw\varepsilon}x(\tau)R_0 + \lambda e^{-jw\varepsilon}h(w,\varepsilon)R_0 + \\ \qquad + \left(\lambda h(w,\varepsilon) - \mu r_0 - \mu r_2 - \lambda\right) R_1. \end{cases} \tag{5}$$

As $\varepsilon \to 0$, we have $\lim\limits_{\varepsilon\to 0} h(w,\varepsilon) = 1$ and system (5) reduces to a single equation

$$-(x(\tau) + \lambda)R_0 + (\mu r_0 + \mu r_2)R_1 = 0. \tag{6}$$

Equation (6) with the normalization condition $R_0 + R_1 = 1$ give R_0 and R_1 as functions of x

$$R_0(x) = \frac{\mu r_0 + \mu r_2}{x + \lambda + \mu r_0 + \mu r_2}, \; R_1(x) = \frac{x + \lambda}{x + \lambda + \mu r_0 + \mu r_2}. \tag{7}$$

We summarize the equations of system (5) and obtain

$$jwx'(\tau) = \left(x(\tau)\frac{e^{-jw\varepsilon} - 1}{\varepsilon} + \lambda\frac{e^{-jw\varepsilon}h(w,\varepsilon) - 1}{\varepsilon}\right) R_0(x) + \\ + \left(\mu r_2\frac{e^{jw\varepsilon} - 1}{\varepsilon} + \lambda\frac{h(w,\varepsilon) - 1}{\varepsilon}\right) R_1(x).$$

As $\varepsilon \to 0$ we get $x'(\tau) = \left(-x(\tau) + \lambda\left(\bar{\nu} - 1\right)\right) R_0(x) + \left(\mu r_2 + \lambda\bar{\nu}\right) R_1(x)$.

We denote by $a(x)$ the right side of the last equality

$$a(x) = \left[\lambda\left(\bar{\nu} - 1\right) - x\right] R_0(x) + \left(\lambda\bar{\nu} + \mu r_2\right) R_1(x). \tag{8}$$

It will be shown below that the function $a(x)$ is the transfer coefficient of some diffusion process approximating the number of customers in orbit.

4. The second stage of asymptotic. A diffusion coefficient

We substitute

$$H_n(u,t) = H_n^{(2)}(u,t)\exp\left\{j\frac{u}{\sigma}x(\sigma t)\right\}, \quad n = 0,1$$

in the system (2) and the equation (3). Here $H_n^{(2)}(u,t)$ is the characteristic function of the centered random variable $i(t) - x(\sigma t)/\sigma$. Then we obtain a system of equations for $H_n^{(2)}(u,t)$ in the form

$$\frac{\partial H_0^{(2)}(u,t)}{\partial t} + jux'(\sigma t)H_0^{(2)}(u,t) = \sigma j\frac{\partial H_0^{(2)}(u,t)}{\partial u} - \\ - (x(\sigma t)+\lambda)H_0^{(2)}(u,t) + \left(\mu r_0 + \mu r_2 e^{ju}\right)H_1^{(2)}(u,t);$$

$$\frac{\partial H_1^{(2)}(u,t)}{\partial t} + jux'(\sigma t)H_1^{(2)}(u,t) = -\sigma j e^{-ju}\frac{\partial H_0^{(2)}(u,t)}{\partial u} + \\ + \left(x(\sigma t) + \lambda h(u)\right)e^{-ju}H_0^{(2)}(u,t) + \\ + \left(\lambda h(u) - \lambda - \mu R_0 - \mu R_2\right)H_1^{(2)}(u,t);$$

$$\frac{\partial H^{(2)}(u,t)}{\partial t} + jux'(\sigma t)H^{(2)}(u,t) = \sigma j\left(1-e^{-ju}\right)\frac{\partial H_0^{(2)}(u,t)}{\partial u} + \\ + \left(x(\sigma t)\left(e^{-ju}-1\right) + \lambda\left(h(u)e^{-ju}-1\right)\right)H_0^{(2)}(u,t) + \\ + \left(\mu r_2\left(e^{ju}-1\right) + \lambda\left(h(u)-1\right)\right)H_1^{(2)}(u,t).$$

We denote $\sigma = \varepsilon^2$ and make a replacement

$$\tau = \varepsilon^2 t, \quad u = \varepsilon w, \quad H_n^{(2)}(u,t) = F_n^{(2)}(w,\tau,\varepsilon),$$

then we get the system

$$\begin{cases} \varepsilon^2\dfrac{\partial F_0^{(2)}(w,\tau,\varepsilon)}{\partial\tau} + j\varepsilon w a(x)F_0^{(2)}(w,\tau,\varepsilon) = j\varepsilon\dfrac{\partial F_0^{(2)}(w,\tau,\varepsilon)}{\partial w} - \\ \quad - (x+\lambda)F_0^{(2)}(w,\tau,\varepsilon) + \left(\mu r_0 + \mu r_2 e^{j\varepsilon w}\right)F_1^{(2)}(w,\tau,\varepsilon); \\ \varepsilon^2\dfrac{\partial F_1^{(2)}(w,\tau,\varepsilon)}{\partial\tau} + j\varepsilon w a(x)F_1^{(2)}(w,\tau,\varepsilon) = -j\varepsilon e^{-j\varepsilon w}\dfrac{\partial F_0^{(2)}(w,\tau,\varepsilon)}{\partial w} + \\ \quad + \left(x+\lambda h(\varepsilon w)\right)e^{-j\varepsilon w}F_0^{(2)}(w,\tau,\varepsilon) + \\ \quad + \left(\lambda h(\varepsilon w) - \lambda - \mu r_0 - \mu r_2\right)F_1^{(2)}(w,\tau,\varepsilon) \end{cases} \tag{9}$$

and equation

$$\varepsilon^2\frac{\partial F^{(2)}(w,\tau,\varepsilon)}{\partial\tau}+j\varepsilon w a(x,\tau)F^{(2)}(w,\tau,\varepsilon)= \\ =\left(x(\tau)\left(e^{-j\varepsilon w}-1\right)+\lambda\left(h(\varepsilon w)e^{-j\varepsilon w}-1\right)\right)F_0^{(2)}(w,\tau,\varepsilon)+ \\ +j\varepsilon\left(1-e^{-j\varepsilon w}\right)\frac{\partial F_0^{(2)}(w,\tau,\varepsilon)}{\partial w}+ \\ +\left(\mu r_2\left(e^{j\varepsilon w}-1\right)+\lambda\left(h(\varepsilon w)-1\right)\right)F_1^{(2)}(w,\tau,\varepsilon). \quad (10)$$

We write the solution $F_n^{(2)}(w,\tau,\varepsilon)$, $n=0,1$ in the form

$$F_n^{(2)}(w,\tau,\varepsilon)=\Phi(w,\tau)\left(R_n+j\varepsilon w F_n\right)+O(\varepsilon^2) \quad (11)$$

and expand $e^{\pm j\varepsilon w}$, $h(\varepsilon w)$ in Taylor series up to the first order of ε in system (9), and up to the second order in equation (10). We substitute (11) into (9), (10) and take into account equations (6), (8), then we can write

$$\begin{aligned} j\varepsilon w a(x)R_0 &= -j\varepsilon w(x+\lambda)f_0+j\varepsilon w\mu r_2 R_1+j\varepsilon w\left(\mu r_0+\mu r_2\right)f_1+ \\ &\quad +j\varepsilon R_0\frac{1}{\Phi(w,\tau)}\frac{\partial\Phi(w,\tau)}{\partial w}+O(\varepsilon^2); \\ j\varepsilon w a(x)R_1 &= j\varepsilon w\left(\lambda\bar{\nu}-\lambda-x\right)R_0+j\varepsilon w(x+\lambda)f_0+j\varepsilon w\lambda\bar{\nu}R_1- \\ &\quad -j\varepsilon w\left(\mu r_0+\mu r_2\right)f_1-j\varepsilon R_0\frac{1}{\Phi(w,\tau)}\frac{\partial\Phi(w,\tau)}{\partial w}+O(\varepsilon^2); \end{aligned} \quad (12)$$

and

$$\varepsilon^2\frac{\partial\Phi(w,\tau)}{\partial\tau}+(j\varepsilon w)^2 a(x)\Phi(w,\tau)f=(j\varepsilon w)^2\left[\left(\lambda\nu_2-2\lambda\bar{\nu}+\lambda+x\right)\frac{R_0}{2}+\right. \\ \left.+\left(\lambda\bar{\nu}-\lambda-x\right)f_0+\left(\lambda\nu_2+\mu r_2\right)\frac{R_1}{2}+\left(\lambda\bar{\nu}+\mu r_2\right)f_1\right]\Phi(w,\tau)+ \\ +(j\varepsilon w)^2\frac{R_0}{w}\frac{\partial\Phi(w,\tau)}{\partial w}+O(\varepsilon^3), \quad (13)$$

where $\nu_2=\sum\limits_{\nu=1}^{\infty}\nu^2 q_\nu$.

After simple transformations using (8), two equations of system (12) are reduced to a single equation

$$-(x+\lambda)f_0+\left(\mu r_0+\mu r_2\right)f_1=a(x)R_0(x)-\mu r_2 R_1(x)-\frac{R_0(x)}{w\Phi(w,\tau)}\frac{\partial\Phi(w,\tau)}{\partial w}.$$

Solution we find in the form

$$f_n=C\cdot R_n(x)+g_n-\varphi_n\frac{1}{w\Phi(w,\tau)}\frac{\partial\Phi(w,\tau)}{\partial w}. \quad (14)$$

Here $C \cdot R_n(x)$ is the general solution of the homogeneous equation due to (6), g_n is the solution of the equation

$$-(x+\lambda)g_0 + (\mu r_0 + \mu r_2)\, g_1 = a(x)R_0(x) - \mu r_2 R_1(x), \tag{15}$$

and φ_n satisfies the equation

$$-(x+\lambda)\frac{(-\varphi_0)}{w\Phi(w,\tau)}\frac{\partial\Phi(w,\tau)}{\partial w} + (\mu r_0 + \mu r_2)\,\frac{(-\varphi_1)}{w\Phi(w,\tau)}\frac{\partial\Phi(w,\tau)}{\partial w} = \\ = -\frac{R_0(x)}{w\Phi(w,\tau)}\frac{\partial\Phi(w,\tau)}{\partial w}.$$

or

$$-(x+\lambda)\varphi_0 + (\mu r_0 + \mu r_2)\,\varphi_1 = R_0(x). \tag{16}$$

Differentiating (6) with respect to x and comparing with (16), we note that $\varphi_0 = \dfrac{\partial R_0(x)}{\partial x}$, $\varphi_1 = \dfrac{\partial R_1(x)}{\partial x}$, $\varphi_0 + \varphi_1 = 0$.

Then, taking into account (7), we obtain

$$\varphi_0 = -\frac{\mu(r_0+r_2)}{(x+\lambda+\mu(r_0+r_2))^2}, \quad \varphi_1 = -\varphi_0. \tag{17}$$

Similarly, we set $g_0 + g_1 = 0$, then from equation (15)

$$g_1 = \frac{aR_0(x) - \mu r_2 R_1(x)}{x+\lambda+\mu r_0+\mu r_2}, \quad g_0 = -g_1. \tag{18}$$

The equation (13) can be written as

$$\frac{\partial\Phi(w,\tau)}{\partial\tau} + (jw)^2 a(x)\Phi(w,\tau)f = (jw)^2\left[(\lambda\nu_2 - 2\lambda\bar{\nu} + \lambda + x)\,\frac{R_0(x)}{2} + \right. \\ + (\lambda\bar{\nu} - \lambda - x)\,f_0 + (\lambda\nu_2 + \mu r_2)\,\frac{R_1(x)}{2} + \left.(\lambda\bar{\nu} + \mu r_2)\,f_1\right]\Phi(w,\tau) + \\ + (jw)^2\frac{R_0(x)}{w}\frac{\partial\Phi(w,\tau)}{\partial w}.$$

We substitute solution (14) into it and, taking into account (8), (17), (18), we obtain

$$\frac{\partial\Phi(w,\tau)}{\partial\tau} = w\frac{\partial\Phi(w,\tau)}{\partial w}\left[(\lambda\bar{\nu} - \lambda - x)\,\varphi_0 + (\lambda\bar{\nu} + \mu r_2)\,\varphi_1 - R_0(x)\right] + \\ + (jw)^2\left[(\lambda\bar{\nu} - \lambda - x)\,g_0 + (\lambda\bar{\nu} + \mu r_2)\,g_1 + (\lambda\nu_2 - 2\lambda\bar{\nu} + \lambda + x)\,\frac{R_0(x)}{2} + \right. \\ \left. + (\lambda\nu_2 + \mu r_2)\,\frac{R_1(x)}{2}\right]\Phi(w,\tau). \tag{19}$$

We denote

$$b(x) = (\lambda\nu_2 - 2\lambda\bar{\nu} + \lambda + x)\, R_0(x) + (\lambda\nu_2 + \mu r_2)\, R_1(x) + \\ + 2\,(\mu r_2 + \lambda + x)\, g_1(x). \quad (20)$$

It will be shown below that the function $b(x)$ is the diffusion coefficient of some diffusion process approximating the number of customers in orbit. Then, taking into account (8), (17), equation (19) can be written in the form

$$\frac{\partial\Phi(w,\tau)}{\partial\tau} = w\frac{\partial\Phi(w,\tau)}{\partial w}a'(x) + \frac{(jw)^2}{2}\Phi(w,\tau)b(x). \quad (21)$$

5. The third stage of asymptotic. A diffuse approximation

The inverse Fourier transform $\Phi(w,\tau) = \int\limits_{-\infty}^{\infty} e^{jwy}P(y,\tau)dy$ converts an equation (21) for the characteristic functions to the equation for the probability density $P(y,\tau)$.

Given the relationship

$$w\frac{\partial\Phi(w,\tau)}{\partial w} = -\int\limits_{-\infty}^{\infty} e^{jwy}(yP(y,\tau))'dy,$$

$$(jw)^2\Phi(w,\tau) = \int\limits_{-\infty}^{\infty} e^{jwy}\frac{\partial^2 P(y,\tau)}{\partial y^2}dy,$$

we obtain the equation

$$\frac{\partial P(y,\tau)}{\partial\tau} = -a'(x)\frac{\partial\,(yP(y,\tau))}{\partial y} + \frac{b(x)}{2}\frac{\partial^2 P(y,\tau)}{\partial y^2}.$$

The resulting equation is the Fokker–Planck equation for the probability density of some diffusion process $y(\tau)$ with transfer coefficient $a'(x)y$ and diffusion coefficient $b(x)$. Thus, the process $y(\tau)$ is a solution of the stochastic differential equation

$$dy(\tau) = a'(x)y(\tau)d\tau + \sqrt{b(x)}d\omega(\tau),$$

where $\omega(\tau)$ is a Wiener process.

We introduce a diffusion process $z(\tau) = x(\tau) + \varepsilon y(\tau)$, where the function $x(\tau)$ is a solution of the ordinary differential equation $dx(\tau) = a(x)d\tau$. Then the diffusion process $z(\tau)$ is a solution of the following stochastic differential equation

$$dz(\tau) = [a(x) + \varepsilon a'(x)y(\tau)]\,d\tau + \varepsilon\sqrt{b(x)}d\omega(\tau).$$

We consider the right hand side of the resulting stochastic differential equation

$$a(x) + \varepsilon a'(x)y = a(x + \varepsilon y) + O(\varepsilon^2) = a(z) + O(\varepsilon^2),$$

$$\varepsilon\sqrt{b(x)} = \varepsilon\sqrt{b(x + \varepsilon y - \varepsilon y)} = \varepsilon\sqrt{b(z - \varepsilon y)} = \varepsilon\sqrt{b(z)} + O(\varepsilon^2)$$

and assume that the terms $O(\varepsilon^2)$ do not contribute significantly to the solution and can be neglected. Then we obtain a stochastic differential equation of the form

$$dz(\tau) = a(z)d\tau + \varepsilon\sqrt{b(z)}d\omega(\tau).$$

We denote by the probability density of the diffusion process $z(\tau)$ as

$$\Pi(z, \tau) = \frac{\partial P\{z(\tau) < z\}}{\partial z}$$

and write the Fokker–Planck equation for this distribution

$$\frac{\partial \Pi(z, \tau)}{\partial \tau} = -\frac{\partial a(z)\Pi(z, \tau)}{\partial z} + \frac{\varepsilon^2}{2}\frac{\partial^2 b(z)\Pi(z, \tau)}{\partial z^2}.$$

The inverse replacement $\sigma = \varepsilon^2$ leads to the equation for stationary probability distribution of diffusion process $z(\tau)$

$$-(a(z)\Pi(z))' + \frac{\sigma}{2}(b(z)\Pi(z))'' = 0,$$

$$(b(z)\Pi(z))' = \frac{2}{\sigma}a(z)\Pi(z).$$

To solve this equation we introduce replacement of variables

$$G(z) = b(z)\Pi(z),$$

and obtain the equation

$$G'(z) = \frac{2}{\sigma}\frac{a(z)}{b(z)}G(z),$$

then the solution is written in the form

$$G(z) = C\exp\left\{\frac{2}{\sigma}\int_0^z \frac{a(x)}{b(x)}dx\right\}.$$

Inverse replacement leads to

$$\Pi(z) = \frac{C}{b(z)}\exp\left\{\frac{2}{\sigma}\int_0^z \frac{a(x)}{b(x)}dx\right\}.$$

On the basis of obtained probability density function we construct the diffusion approximation by formula

$$PD(i) = \frac{\Pi(i\sigma)}{\sum\limits_{n=0}^{\infty} \Pi(n\sigma)}. \tag{22}$$

6. Numerical results

We determine the applicability of the obtained approximation by comparing the asymptotic distribution (22) with the steady state distribution $P(i)$ obtained when solving the system (1) by the matrix method. We consider different values of the parameter σ. To compare two probability distributions, we use the Kolmogorov distance

$$\Delta_1 = \max_{0 \le n < \infty} \left| \sum_{i=0}^{n} (P(i) - PD(i)) \right|. \tag{23}$$

We consider following system parameters $\lambda = 1$, $r_0 = 0.5$, $r_1 = 0.3$, $r_2 = 0.2$, $q_1 = 0.5$, $q_2 = 0.3$, $q_3 = 0.1$, $q_4 = 0.1$. We introduce the system loading parameter $\rho = \frac{\lambda\bar{\nu}}{\mu r_0}$. It defines the value of the parameter μ. We take $\Delta = 0.05$ as a threshold value.

Table 1 presents Kolmogorov distances Δ_1 calculated by formula (23), table 2 presents Kolmogorov distances Δ_2 calculated for the Gaussian approximation obtained in [6]. Bold in the tables are the values that correspond to a satisfactory approximation accuracy. It can be concluded that the accuracy of diffusion approximation increases with decreasing the parameter σ and increasing the system load ρ, and the accuracy of Gaussian approximation decreases with high system load. In addition, the accuracy of the diffusion approximation is higher than the accuracy of the Gaussian approximation.

Table 1

Kolmogorov distance Δ_1

Δ_1	$\sigma = 2$	$\sigma = 1$	$\sigma = 0.5$	$\sigma = 0.1$	$\sigma = 0.05$
$\rho = 0.2$	0.135	0.089	0.050	**0.016**	**0.012**
$\rho = 0.5$	0.094	0.060	**0.035**	**0.013**	**0.009**
$\rho = 0.7$	0.059	**0.036**	**0.021**	**0.009**	**0.006**
$\rho = 0.9$	**0.019**	**0.011**	**0.007**	**0.003**	**0.002**

Table 2

Kolmogorov distance Δ_2

Δ_2	$\sigma = 2$	$\sigma = 1$	$\sigma = 0.5$	$\sigma = 0.1$	$\sigma = 0.05$
$\rho = 0.2$	0.221	0.152	0.086	**0.018**	**0.013**
$\rho = 0.5$	0.162	0.105	**0.047**	**0.027**	**0.019**
$\rho = 0.7$	0.175	0.108	**0.045**	**0.039**	**0.027**
$\rho = 0.9$	0.187	0.109	0.084	0.057	**0.040**

7. Conclusions

The mathematical model of the system $M^{[n]}/M/1$ with an incoming batch Poisson flow and feedback is constructed. The system of equations for probability distribution of the number of customers in orbit is present.

A diffusion approximation of the probability distributions of the number of customers in orbit is obtained. The asymptotic condition is growing average waiting time in orbit. The accuracy of the approximation is determined using the Kolmogorov distance in comparison with the steady state probability distribution obtained by the matrix method. Numerical examples are given for different values of the system parameters, the accuracy of the diffusion approximation and the Gaussian approximation is compared. It is shown that the accuracy of the diffusion approximation is higher than the accuracy of the Gaussian approximation.

References

[1] T. Phung-Duc, *Retrial queueing models: A survey on theory and applications*, 2019. arXiv: 1906.09560.

[2] J. Kim and B. Kim, "A survey of retrial queueing systems," *Annals of Operations Research*, vol. 247, no. 1, pp. 3–36, 2016. DOI: 10.1007/s10479-015-2038-7.

[3] Y. Barlas and O. Özgün, "Queuing systems in a feedback environment: Continuous versus discrete-event simulation," *Journal of Simulation*, vol. 12, no. 2, pp. 144–161, 2018. DOI: 10.1080/17477778.2018.1465153.

[4] A. Melikov, V. Divya, and S. Aliyeva, "Analyses of feedback queue with positive server setup time and impatient calls," in *Information technologies and mathematical modelling (ITTM-2020)*, Proceedings of the 19th International Conference named after A. F. Terpugov (2020 December, 2–5), Tomsk: Scientific Technology Publishing House, 2021, pp. 77–81.

[5] N. Singla and H. Kaur, "A two-state retrial queueing model with feedback and balking," *Reliability: Theory & Applications*, vol. 16, no. SI 2 (64), pp. 142–155, 2021. DOI: 10.24412/1932-2321-2021-264-142-155.

[6] A. A. Nazarov, S. V. Rozhkova, and E. Y. Titarenko, "Asymptotic analysis of RQ-system with feedback and batch Poisson arrival under the condition of increasing average waiting time in orbit," *Communications in Computer and Information Science*, vol. 1337, pp. 327–339, 2020. DOI: 10.1007/978-3-030-66242-4_26.

[7] A. A. Moiseev, A. A. Nazarov, and S. V. Paul, "Asymptotic diffusion analysis of multi-server retrial queue with hyper-exponential service," *Mathematics*, vol. 8, no. 4, 2020. DOI: 10.3390/math8040531.

For citation:

A. A. Nazarov, S. V. Rozhkova, E. Yu. Titarenko, Asymptotic diffusion analysis of the retrial queuing system with feedback and batch Poisson arrival, Discrete and Continuous Models and Applied Computational Science 31 (3) (2023) 205–217. DOI: 10.22363/2658-4670-2023-31-3-205-217.

Information about the authors:

Nazarov, Anatoly A. — Doctor of Technical Sciences, Professor of Department of Probability Theory and Mathematical Statistics, Institute of Applied Mathematics and Computer Science, National Research Tomsk State University (e-mail: nazarov.tsu@gmail.com, ORCID: https://orcid.org/0000-0002-5097-5629)

Rozhkova, Svetlana V. — Doctor of Physical and Mathematical Sciences, Professor of Department of Mathematics and Computer Science, School of Core Engineering Education, National Research Tomsk Polytechnic University, professor of Department of Probability Theory and Mathematical Statistics, Institute of Applied Mathematics and Computer Science, National Research Tomsk State University (e-mail: rozhkova@tpu.ru, phone: +7(3822)701777-6898, ORCID: https://orcid.org/0000-0002-8888-9291)

Titarenko, Ekaterina Yu. — Lecturer of Mathematics and Computer Science, School of Core Engineering Education, National Research Tomsk Polytechnic University (e-mail: teu@tpu.ru, phone: +7(3822)701777-1155, ORCID: https://orcid.org/0000-0002-0478-8232)

УДК 519.872
DOI: 10.22363/2658-4670-2023-31-3-205-217
EDN: LACMZU

Асимптотически диффузионный анализ RQ-системы с обратными связями и неординарным входящим потоком

А. А. Назаров[1], **С. В. Рожкова**[1,2], **Е. Ю. Титаренко**[2]

[1] *Институт прикладной математики и компьютерных наук, Томский государственный университет пр. Ленина, д. 36, Томск, 634050, Россия*
[2] *Отделение математики и информатики школы базовой инженерной подготовки, Томский политехнический университет, ул. Советская, д. 73 стр.1, Томск, 634050, Россия*

Аннотация. В работе исследована $M^{[n]}/M/1$ RQ-система с неординарным пуассоновским входящим потоком. Заявки на вход системы поступают группами. В каждый момент времени обслуживается не более одной заявки, остальные попадают на орбиту. Заявка, обслуживание которой завершено, либо покидает систему, либо повторно поступает на обслуживание, либо переходит на орбиту. Методом асимптотически диффузионного анализа при асимптотическом условии растущего среднего времени ожидания на орбите построена аппроксимация распределения вероятностей числа заявок на орбите. Показано, что точность диффузионной аппроксимации превышает точность гауссовской аппроксимации.

Ключевые слова: система массового обслуживания, RQ-система, неординарный поток, обратная связь, асимптотически-диффузионный анализ

Discrete & Continuous Models & Applied Computational Science
ISSN 2658-7149 (online), 2658-4670 (print)
2023, 31 (3) 218–227
http://journals.rudn.ru/miph

Research article

UDC 519.872:519.217
PACS 07.05.Tp, 02.60.Pn, 02.70.Bf
DOI: 10.22363/2658-4670-2023-31-3-218-227
EDN: YENIDI

Numerical integration of the Cauchy problem with non-singular special points

Aleksandr A. Belov[1, 2], **Igor V. Gorbov**[1]

[1] *M. V. Lomonosov Moscow State University,*
1, bld. 2, Leninskie Gory, Moscow, 119991, Russian Federation
[2] *Peoples' Friendship University of Russia (RUDN University),*
6, Miklukho-Maklaya St., Moscow, 117198, Russian Federation

(received: July 28, 2023; revised: August 28, 2023; accepted: September 8, 2023)

Abstract. Solutions of many applied Cauchy problems for ordinary differential equations have one or more multiple zeros on the integration segment. Examples are the equations of special functions of mathematical physics. The presence of multiples of zeros significantly complicates the numerical calculation, since such problems are ill-conditioned. Round-off errors may corrupt all decimal digits of the solution. Therefore, multiple zeros should be treated as special points of the differential equations. In the present paper, a local solution transformation is proposed, which converts the multiple zero into a simple one. The calculation of the latter is not difficult. This makes it possible to dramatically improve the accuracy and reliability of the calculation. Illustrative examples have been carried out, which confirm the advantages of the proposed method.

Key words and phrases: ordinary differential equations, Cauchy problem, multiple zero, solution transformation

1. Introduction

Consider the Cauchy problem for an ordinary differential equation (ODE)

$$du/dt = f(u,t), \quad u(0) = u^0. \tag{1}$$

The solution of many such problems has one or more multiples of zeros inside the integration segment. Examples are special functions: elliptic Weierstrass functions [1], θ-function [2], derivatives of cylindrical functions [3], and a number of others.

To calculate them, power series, Fourier series or direct numerical integration of the original equation [2] are used. The latter method seems to be the most versatile. However, the numerical calculation of such problems faces

a typical difficulty. If the grid node exactly coincides with the position of the solution zero and the order of accuracy of the scheme does not exceed the multiplicity of the zero, then the further numerical solution identically equals and calculation becomes impossible. If the grid node does not coincide with the soluton zero, but is close to it, then the numerical solution becomes so small in absolute magnitude that it turns out to be comparable to unit round-off errors.

After passing a multiple of zero, the integral curves diverge rapidly, so the contribution of rounding errors increases by many orders of magnitude. Thus, passing a multiple of zero "removes" several significant digits from the solution. The more multiples of zeros fall on the integration segment, the greater the loss of accuracy. Such tasks are called ill-conditioned [4].

Therefore, we propose to consider multiple zeros in the solution of differential equations as special points along with poles and root singularities. We call them non-singular special points.

In the present paper, a new method for calculating problems with non-singular features is proposed. It consists of two stages:

1) numerical detection of the nearest zero, calculation of its position and multiplicity;
2) local transformation of the solution, which converts a multiple zero into a simple one. The calculation of such a solution is not difficult.

The method is generalized to ODE systems. Examples illustrating the advantages of the proposed approach are given.

2. Detection of the nearest zero

Let the nearest zero of the solution $u(t)$ be located at the point T and has a multiplicity q. The values of q and T are unknown in advance. Let us introduce the grid t_n, $0 \leqslant n \leqslant N$, $h = t_{n+1} - t_n$ for the independent variable. Let the calculation be carried out according to some difference scheme. The numerical solution is denoted by u_n. Obviously, the algorithm for investigating the nearest zero can use only those values of u_n for which $t_n < T$. Otherwise, the accuracy of such a study deteriorates dramatically.

Earlier in [5, 6], an algorithm for numerical detection of the nearest pole in the solution of the ODE was proposed. A zero can be considered as a pole of negative order. Therefore, we can apply this technique to the study of zeros. Let us describe the corresponding procedure. Near zero, the representation is valid

$$u = C_q(T-t)^q + C_{q+1}(T-t)^{q+1} + \dots . \tag{2}$$

Let us neglect the second and subsequent terms and differentiate this equality. Taking into account (1), we get

$$f = -\frac{qu}{T-t}. \tag{3}$$

Let us write (3) in nodes n and $n+1$. We obtain a system of equations with respect to the quantities q and T. Its solution has the form

$$q_n = \frac{t_n - t_{n+1}}{u_n/f_n - u_{n+1}/f_{n+1}}, \quad T_n = q\frac{u_n}{f_n} + t_n. \tag{4}$$

Although the exact value of q is an integer, the calculated q_n turns out to be a float-point number.

The formulas (4) are actually a difference scheme for q and T. Its error consists of two factors: the error of the original difference scheme for the problem (1) and the error introduced by discarding the second and subsequent terms in (2). The first factor can be reduced by conducting a global thickening of the grid $h \to 0$. The second factor decreases with the tendency of $t_n \to T$ even if the grid step is fixed.

It is not difficult to show that if the calculated values of q_n and T_n tend to be constant when the number of the current node n increases, then the detected singular point is a multiple of zero. The justification of this statement reproduces almost verbatim the proof of Theorem 1 from [7].

3. Transformation of the solution

w-transformation. Suppose, during the calculation using the procedure described above, a multiple zero of the solution $u(t)$ is detected. This means that for some n, the next change in the calculated q_n and T_n is quite small: $|q_n - q_{n-1}| < \varepsilon$, $|T_n - T_{n-1}| < \varepsilon$, where ε is some small number. The number of the node where this condition is met is denoted by n_*.

Round q_{n_*} to an integer and introduce a new unknown function

$$w = \operatorname{sign}(u)|u|^{1/q}. \tag{5}$$

It is not difficult to make sure that $w(t)$ satisfies the problem

$$\frac{dw}{dt} = \frac{w^{1-q}}{q} f(w^q, t), \quad w(t_{n_*}) = \operatorname{sign}(u_{n_*})|u_{n_*}|^{1/q}. \tag{6}$$

The function w has a simple zero at the point T. Numerical calculation of such a solution is not difficult.

Starting from the moment t_{n_*} we solve the problem (6) according to the same scheme as the original problem. Simultaneously, at each step, we calculate the solution $u_n = (w_n)^q$ both before and after the zero. After passing w through zero, we return to the calculation of the original problem (1). Similarly, the calculation of the second and subsequent zeros is carried out.

τ-transformation. The geometric interpretation of the transformation described above is that the multiple zero of the function u becomes a simple zero of the function w. The same result can be achieved by introducing a transformation of the independent variable instead of the solution.

Let us calculate q (rounded to an integer) and T. Let us introduce a new argument $\tau = (T-t)^q$. The solution $u(\tau)$ has a simple zero at the point T.

In the new argument, the equation (1) takes the form

$$\frac{du}{d\tau} = -\frac{1}{q}\tau^{1/q-1} f(u, T - \tau^{1/q}). \tag{7}$$

The calculation is carried out in the same way as described in the previous paragraph.

4. Generalizations

ODE systems. It is easy to generalize the described approach to the case of an ODE system of the order of J

$$\frac{d\mathbf{u}}{dt} = \mathbf{f}(\mathbf{u}, t), \quad \mathbf{u}(0) = \mathbf{u}^0, \tag{8}$$

where $\mathbf{u} = \{u^1, u^2, \dots, u^J\}$, $\mathbf{f} = \{f^1, f^2, \dots, f^J\}$.

Let several components of the solution contain multiple zeros located in the general case at different points. Then a representation similar to (2) is valid for each of these components. For each component of the solution, we conduct the study described in section 2. Let the nearest zero be located in the component u^k; it corresponds to the moment of time T^k and has the order q^k. Let us introduce a replacement (5) for the k-th component without changing other components. The resulting system takes the form

$$\begin{aligned} \frac{dw^k}{dt} &= \frac{1}{q^k}[w^k]^{1-q^k} f^k(u^1, u^2, \dots, u^{k-1}, [w^k]^{q_k}, u^{k+1}, \dots, u^J), \\ \frac{du^j}{dt} &= f^j(u^1, u^2, \dots, u^{k-1}, [w^k]^{q^k}, u^{k+1}, \dots, u^J), \quad 1 \leqslant j \leqslant J, \quad j \neq k. \end{aligned} \tag{9}$$

Let us calculate the system (9) until the component w^k passes through zero. Simultaneously with w^k at each step we calculate $u^k = [w^k]^{q^k}$. Then we return to the original system (8) and integrate it, simultaneously conducting a numerical study of zeros in each component. When the nearest multiple zero of one of the components is detected, we introduce a system similar to (9), etc.

Multiple constant. In addition to multiple zeros, similar difficulties are presented by points where the solution itself is different from zero, and several first derivatives are zero. Such features are natural to denote as multiple constants. In the vicinity of such a point, the solution is represented as

$$u(t) = A + C_q(T - t)^q + \dots, \tag{10}$$

where $A \neq 0$. The proposed approach can be applied directly to such problems if the value of A is known exactly. To do this, it is enough to make a transformation

$$w = A + \operatorname{sign}(u)|u|^{1/q}. \tag{11}$$

The case when A is unknown in advance is particularly difficult. We have attempted to construct various difference schemes for calculating A by analogy with 2. However, the accuracy of this calculation was insufficient to construct a transformation of the form (11). Therefore, we leave the case of the unknown A outside the scope of this work.

5. Validation

Test example. As test examples, it is advisable to choose problems with a known exact solution, which is expressed in elementary functions. This allows a particularly thorough verification of the numerical method.

Let us set the exact solution

$$u_{\text{ex}}(t) = \cos^q(\pi t + \pi/4). \tag{12}$$

It has zeros of multiplicity q at points $T_k = 1/4 + k$, $k = 1, 2, \ldots$. Let us construct a differential equation for it. There are different ways to do this. However, an equation with the right-hand side depending only on t is of no interest, since it is solved by quadrature. On the other hand, the right-hand side, which depends only on u, also appears to be a special case. Therefore, we consider a non-autonomous equation

$$\frac{du}{dt} = -q\pi |u|^{1-1/q} \sin(\pi t - \pi/4). \tag{13}$$

The initial condition is set according to (12). The integration segment $0 < t < t_{\max}$ is selected so that it contains a specified number of multiples of zeros.

Figure 1 shows the field of integral curves for this problem. This graph illustrates what is said in section 1. The rapid divergence of the integral curves after each multiple of zero is clearly visible. It is also seen that even a relatively small change in the initial condition significantly changes the integral curve.

Along with the equation (13) in the argument "time" t, the corresponding system was considered in the argument "arc length of the integral curve" l [8, 9]. Recall the formulas for the transition to this argument

$$\frac{du}{dl} = \frac{f}{\sqrt{1+f^2}}, \quad \frac{dt}{dl} = \frac{1}{\sqrt{1+f^2}}. \tag{14}$$

It is easy to see that in this argument the vector of the right parts has unit length. It is also known [8] that parameterization through the arc length provides the best conditionality of the problem (in a global sense, i.e. over the entire segment $0 < t < t_{\max}$).

Testing methodology. The calculation of the task (13) or (14) is carried out until the specified time point $t_{\max}$ is reached. Each calculation was carried out on a set of thickening grids: the first grid contained N intervals of length h, the second had $2N$ intervals of length $h/2$, etc. The error of the numerical

solution was calculated on each grid as the difference between numerical and exact solutions

$$\delta_n = u_n - u_{\text{ex}}(t_n). \tag{15}$$

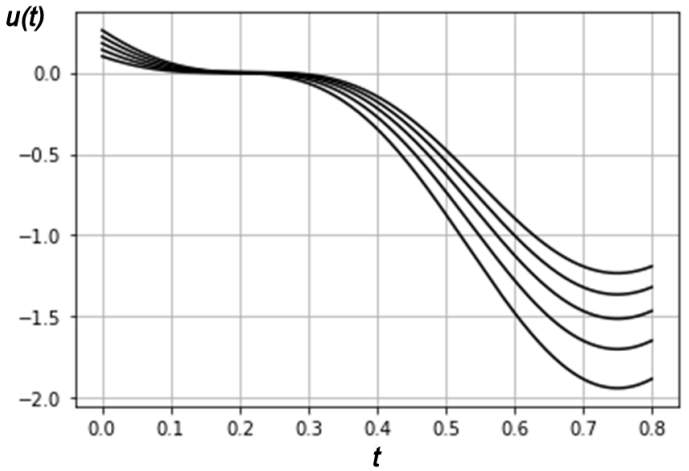

Figure 1. The field of integral curves of the equation (13)

For the problem (14), the exact solution as a function of the arc length is unknown, so we consider the error according to (15), substituting the calculated time points t_n into the exact solution (12).

Method choice. Let us put $t_{\max} = 3\pi/2 \approx 4.7$. Then the segment $0 < t < t_{\max}$ contains 5 zeros of the solution. Let $q = 3$. Let us calculate the problem (13) using an explicit four-stage Runge–Kutta scheme (ERK4) [10] using the proposed approach.

Figure 2 shows the error of the obtained solution depending on the number of grid nodes on a double logarithmic scale. Power convergence $\delta_N \sim N^{-p}$ corresponds to a straight line with a slope of $-p$.

Visually, the error curve decreases and tends to a straight line with a slope of -4. This corresponds to the theoretical 4th order of accuracy of this scheme. On excessively detailed grids, the error reaches the value $\sim 10^{-14}$ and ceases to decrease. This corresponds to the background of rounding errors. It can be seen that they are only 100 times larger than the unit rounding error. This shows the high reliability of the proposed approach.

For comparison, we performed calculations of this problem without using the proposed approach. Various schemes were used: the explicit ERK4 scheme, the explicit-implicit one-step Rosenbrock scheme with complex coefficient CROS [11], implicit optimal backward Runge–Kutta scheme BORK4 [12, 13] and the explicit Dorman–Prince method with automatic step selection DoPri5 [14, 15]. The error obtained in these calculations is also shown in figure 2. It can be seen that the ERK4, CROS and BORK4 schemes without replacement give approximately the same errors. The rate of their descending roughly corresponds to the first order of accuracy, which is sharply different from their theoretical orders of accuracy. The convergence of the DoPri5

method turns out to be faster, but the accuracy cannot be obtained better than 10^{-3}.

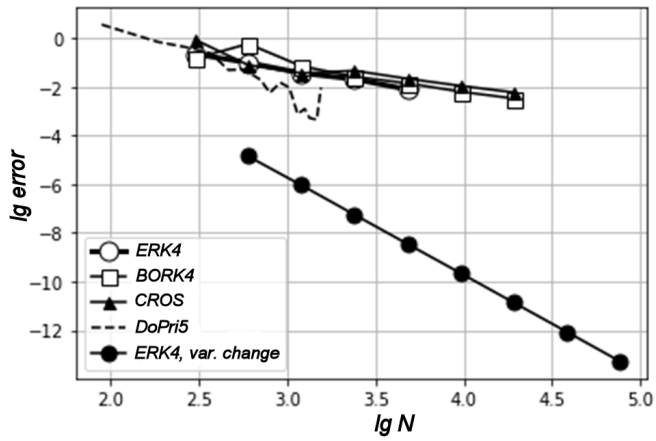

Figure 2. Errors in the test (13)

Thereby, from figure 2 it can be seen that the proposed approach dramatically increases the accuracy and reliability of the calculation. The problem under consideration presents a significant difficulty for classical schemes. However, the proposed approach allows calculations to be carried out even according to explicit schemes and to obtain an accuracy not much higher than the errors of unit round-off error.

Figure 3 shows similar calculations of the problem (14). It is clearly seen that the ERK4 scheme with the proposed replacement implements the theoretical order of accuracy and provides excellent accuracy up to $\sim 10^{-14}$. In calculations without the proposed replacement, all schemes give significantly worse accuracy and do not implement the theoretical order of convergence.

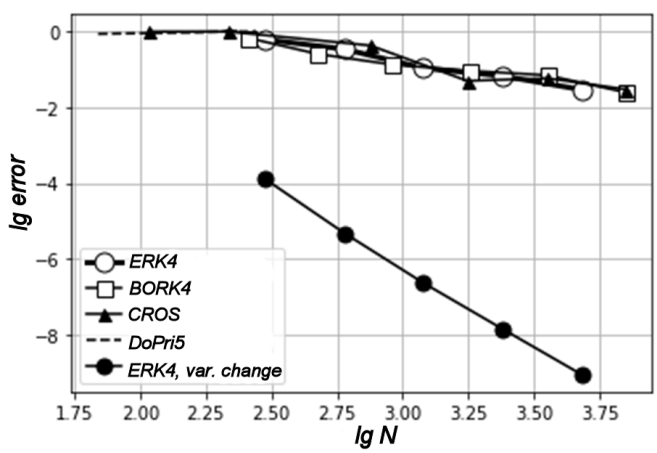

Figure 3. Errors in the test (14)

6. Conclusion

The test calculations have shown that the proposed approach for numerical solution of the Cauchy problems with multiple zeros on the integration segment provides high accuracy and reliability of calculation for a wide class of problems. At the same time, standard approaches demonstrate unsatisfactory accuracy. The simplicity of implementation, the possibility of generalization and use with a large set of numerical schemes make the method convenient for application to applied problems.

Acknowledgments

This work did not receive specific funding.

References

[1] E. Janke, F. Emde, and F. Losch, *Tafeln Horer Functionen*. Stutgart: B. G. Teubner Verlagsgesellschaft, 1960.

[2] *NIST Digital Library of Mathematical Functions*, https://dlmf.nist.gov.

[3] M. K. Kerimov, "Studies on the zeros of Bessel functions and methods for their computation," *Computational Mathematics and Mathematical Physics*, vol. 54, pp. 1337–1388, 2014. DOI: 10.1134/S0965542514090073.

[4] N. N. Kalitkin and P. V. Koryakin, *Numerical methods. Vol.2: Methods of mathematical physics [Chislennye Metody. T.2: Metody matematicheskoi fiziki]*. Moscow: Akademiya, 2013, in Russian.

[5] A. A. Belov, "Numerical detection and study of singularities in solutions of differential equations," *Doklady Mathematics*, vol. 93, no. 3, pp. 334–338, 2016. DOI: 10.1134/S1064562416020010.

[6] A. A. Belov, "Numerical blow-up diagnostics for differential equation solutions," *Computational Mathematics and Mathematical Physics*, vol. 57, no. 1, pp. 122–132, 2017. DOI: 10.1134/S0965542517010031.

[7] A. A. Belov and N. N. Kalitkin, "Numerical integration of a Cauchy problem whose solution has integer-order poles on the real axis," *Differential equations*, vol. 58, pp. 810–833, 2022. DOI: 10.1134/S0012266122060088.

[8] V. I. Shalashilin and E. B. Kuznetsov, *The method of continuation by parameter and the best parametrization [Metod prodolzheniia po parametru i nailuchshaia parametrizatsiia]*. Moscow: Editorial URSS, 1999, in Russian.

[9] E. B. Kuznetsov and S. S. Leonov, "Parametrization of the Cauchy problem for systems of ordinary differential equations with limiting singular points," *Computational Mathematics and Mathematical Physics*, vol. 57, pp. 931–952, 2017. DOI: 10.1134/S0965542517060094.

[10] E. A. Alshina, E. M. Zaks, and N. N. Kalitkin, "Optimal parameters of explicit Runge–Kutta schemes of low orders [Optimalnye parametry iavnykh skhem Runge–Kutty nizkikh poriadkov]," *Math. modeling*, vol. 18, no. 2, pp. 61–71, 2006, in Russian.

[11] H. H. Rosenbrock, "Some general implicit processes for the numerical solution of differential equations," *The Computer Journal*, vol. 5, no. 4, pp. 329–330, 1963. DOI: 10.1093/comjnl/5.4.329.

[12] N. N. Kalitkin and I. P. Poshivaylo, "Inverse Ls-stable Runge–Kutta schemes," *Doklady Mathematics*, vol. 85, pp. 139–143, 2012. DOI: 10.1134/S1064562412010103.

[13] N. N. Kalitkin and I. P. Poshivaylo, "Computations with inverse Runge–Kutta schemes," *Mathematical Models and Computer Simulations*, vol. 6, pp. 272–285, 2014. DOI: 10.1134/S2070048214030077.

[14] E. Hairer and G. Wanner, *Solving ordinary differential equations. II. Stiff and differential-algebraic problems*. Berlin, New York: Springer-Verlag, 1996.

[15] L. F. Shampine and M. W. Reichelt, "The Matlab ODE suite," *SIAM Journal on Scientific Computing*, vol. 18, no. 1, pp. 1–22, 1997. DOI: 10.1137/S1064827594276424.

For citation:

A. A. Belov, I. V. Gorbov, Numerical integration of the Cauchy problem with non-singular special points, Discrete and Continuous Models and Applied Computational Science 31 (3) (2023) 218–227. DOI: 10.22363/2658-4670-2023-31-3-218-227.

Information about the authors:

Belov, Aleksandr A. — Candidate of Physical and Mathematical Sciences, Assistant professor of Department of Computational Mathematics and Artificial Intelligence of Peoples' Friendship University of Russia (RUDN University); Researcher of Faculty of Physics, M. V. Lomonosov Moscow State University (e-mail: aa.belov@physics.msu.ru, phone: +7(495)9393310, ORCID: https://orcid.org/0000-0002-0918-9263)

Gorbov, Igor V. — Master's degree student of Faculty of Physics, M. V. Lomonosov Moscow State University (e-mail: garri-g@bk.ru, phone: +7(495)9393310, ORCID: https://orcid.org/0009-0005-5335-6179)

УДК 519.872:519.217
PACS 07.05.Tp, 02.60.Pn, 02.70.Bf
DOI: 10.22363/2658-4670-2023-31-3-218-227
EDN: YENIDI

Численное интегрирование задач Коши с несингулярными особыми точками

А. А. Белов[1, 2], **И. В. Горбов**[1]

[1] *Московский государственный университет им. М. В. Ломоносова, Ленинские горы, д. 1, стр. 2, Москва, 119991, Россия*
[2] *Российский университет дружбы народов, ул. Миклухо-Маклая, д. 6, Москва, 117198, Россия*

Аннотация. Решения многих прикладных задач Коши для обыкновенных дифференциальных уравнений имеют один или несколько кратных нулей на отрезке интегрирования. Примерами являются уравнения специальных функций математической физики. Наличие кратных нулей существенно затрудняет численный расчёт, поскольку такие задачи являются плохо обусловленными. Из-за ошибок округления в решении может не остаться ни одного верного знака. Поэтому кратные нули следует отнести к особым точкам ОДУ. В данной работе предложена локальная замена искомой функции, которая преобразует кратный нуль решения в простой. Расчёт последнего не представляет трудностей. Это позволяет кардинально повысить точность и надёжность расчёта. Проведены иллюстративные примеры, которые подтверждают преимущества предлагаемого метода.

Ключевые слова: обыкновенные дифференциальные уравнения, задача Коши, кратные нули, преобразование решения

Discrete & Continuous Models & Applied Computational Science
ISSN 2658-7149 (online), 2658-4670 (print)
2023, 31 (3) 228–241
http://journals.rudn.ru/miph

Research article

UDC 519.6
PACS 07.05.Tp, 02.60.Pn, 02.70.Bf
DOI: 10.22363/2658-4670-2023-31-3-228-241
EDN: KNQAEY

On a stable calculation of the normal to a surface given approximately

Evgeniy B. Laneev, Obaida Baaj

Peoples' Friendship University of Russia (RUDN University),
6, Miklukho-Maklaya St., Moscow, 117198, Russian Federation

(received: August 17, 2023; revised: August 31, 2023; accepted: September 8, 2023)

Abstract. The paper proposes a stable method for constructing a normal to a surface given approximately. The normal is calculated as the gradient of the function in the surface equation. As is known, the problem of calculating the derivative is ill-posed. In the paper, an approach is adopted to solving this problem as to the problem of calculating the values of an unbounded operator. To construct its stable solution, the principle of minimum of the smoothing functional in Morozov's formulation is used. The normal is obtained in the form of a Fourier series in the expansion in terms of eigenfunctions of the Laplace operator in a rectangle with boundary conditions of the second kind. The functional stabilizer uses the Laplacian, which makes it possible to obtain a normal in the form of a Fourier series that converges uniformly to the exact normal vector as the error in the surface definition tends to zero. The resulting approximate normal vector can be used to solve various problems of mathematical physics using surface integrals, normal derivatives, simple and double layer potentials.

Key words and phrases: ill-posed problem, stable derivative calculation, regularization method, discrete Fourier series

1. Introduction

When solving many problems of mathematical physics, which are boundary value problems for partial differential equations, there is a need to calculate the normal to the surface, in particular, when calculating the normal derivative. For example, when calculating the potentials of a simple and double layer, as well as other surface integrals.

In the case when the surface is known "exactly", that is, for example, it is given by an equation with an exactly known function

$$F(x, y, z) = 0, \tag{1}$$

then the normal (generally speaking, not unit normal) will be calculated up to the sign in the form of the gradient of the function in the equation of the surface

$$\mathbf{n}_1 = \mathrm{grad} F(x, y, z) = \nabla F. \tag{2}$$

In applied problems, a situation may arise when the surface is not known accurately. The error may be related to the measurement error, digitization, or the surface data is the result of modeling, that is, it contains the model error. That is, even in the case when the surface is given by the equation $z = F(x, y)$, where the function F is given analytically, that is, "exactly", such a surface can be considered as "model", approximately describing "real" surface.

In applied problems, a situation may arise when the surface is not known accurately. In the case when the surface is known inaccurately, it becomes necessary to calculate the normal to the surface given approximately.

As follows from (2), the calculation of the normal is related to the calculation of the derivatives of the function in the equation of the surface. As [1] is known, such a problem is ill-posed and in the case when the surface is known approximately, the use of regularizing algorithms is required to obtain its approximate solution.

The problem of calculating the derivative of a function as an ill-posed problem has been considered in many works, for example [2–9] and others. Here, following [10], we will solve the problem of stable differentiation as a problem of calculating the values of an unbounded operator.

2. Problem statement

When solving the problem of constructing a normal vector to a surface, we confine ourselves to considering a surface of the form

$$S = \{(x, y, z) : 0 < x < l_x,\ 0 < y < l_y,\ z = F(x, y)\}, \tag{3}$$

that is, a surface given by the equation

$$z = F(x, y), \quad F \in C^2(\Pi) \tag{4}$$

on a rectangle

$$\Pi = \{(x, y) : 0 < x < l_x,\ 0 < y < l_y\}. \tag{5}$$

As follows from (2), for an exactly given function F, the normal vector is calculated by the formula

$$\mathbf{n}_1 = \mathrm{grad}\,(F(x, y) - z) = \nabla_{xy} F - \mathbf{k}. \tag{6}$$

Let the surface S be given with an error, namely: instead of the exact function F in (3), there is a function F^μ defined on a rectangle Π of the form (5), so

$$\|F^\mu - F\|_{L_2(\Pi)} \leqslant \mu. \tag{7}$$

Let us pose the problem of constructing a uniform approximation to the normal vector to the surface that converges uniformly to the exact one as $\mu \to 0$.

Note that the normal vector is needed to calculate the normal derivative of the function $\dfrac{\partial \varphi}{\partial n} = (\mathbf{n}, \nabla\varphi)$, $\mathbf{n} = \dfrac{\mathbf{n_1}}{n_1}$, as well as when calculating surface integrals to calculate a surface element $d\sigma = n_1(x, y)dxdy$.

3. Constructing a stable solution to the problem

To calculate the normal vector to the surface given by the equation (2), in accordance with (6), it is necessary to calculate the gradient $\nabla_{xy}F$. To obtain a solution of the formulated problem that is stable to the error (7), we use the [11] approach, which consists in the fact that the problem of calculating the gradient $\nabla_{xy}F$ is considered as the problem of calculating the values of an unbounded operator [10]. In contrast to [11], we will consider the Laplacian instead of the gradient as an unbounded operator, which allows us to obtain a uniform approximation for the normal.

As an approximation to the function $\nabla_{xy}F$, computed from the known function F^μ related to the function F by the condition (7), we will consider the gradient of the extremal of the functional

$$N^\beta[W] = \|W - F^\mu\|^2_{L_2(\Pi)} + \beta \|\Delta W\|^2_{L_2(\Pi)}, \quad \beta > 0 \tag{8}$$

in which the squared norm of the Laplacian of the argument of the functional is used as a stabilizer.

We assume that the surface S of the form (3) satisfies the conditions

$$F'_x|_{x=0,l_x} = 0, \quad F'_y|_{y=0,l_y} = 0; \quad F'''_y|_{x=0,l_x} = 0, \quad F'''_y|_{y=0,l_y} = 0. \tag{9}$$

We obtain the Euler equation for the functional (8). To vary the functional, we have

$$\delta N^\beta[W] = 2\,(W - F^\mu, \delta W) + 2\beta(\Delta W, \Delta\delta W). \tag{10}$$

We write the second scalar product in (10) as a double integral

$$\delta N^\beta[W] = 2\,(W - F^\mu, \delta W) + 2\beta \int\limits_0^{l_x}\int\limits_0^{l_y} dxdy \Delta W(x, y)\Delta\delta W(x, y). \tag{11}$$

Separating the second derivatives in the Laplacian and changing the order of integration over the variables x and y, we transform the double integrals by integrating by parts:

$$\int\limits_0^{l_x}\int\limits_0^{l_y} dxdy \Delta W(x, y)\Delta\delta W(x, y) =$$

$$= \int_0^{l_y} dy \int_0^{l_x} dx \Delta W(x,y) \frac{\partial^2}{\partial x^2} \delta W(x,y) + \int_0^{l_x} dx \int_0^{l_y} dy \Delta W(x,y) \frac{\partial^2}{\partial y^2} \delta W(x,y) =$$

$$= \int_0^{l_y} dy \left[\Delta W(x,y) \delta W'_x(x,y) \Big|_{x=0}^{x=l_x} - \int_0^{l_x} dx \frac{\partial}{\partial x} \Delta W(x,y) \frac{\partial}{\partial x} \delta W(x,y) \right] +$$

$$+ \int_0^{l_x} dx \left[\Delta W(x,y) \delta W'_y(x,y) \Big|_{y=0}^{y=l_y} - \int_0^{l_y} dy \frac{\partial}{\partial y} \Delta W(x,y) \frac{\partial}{\partial y} \delta W(x,y) \right]. \quad (12)$$

Since the extremal must satisfy the same boundary conditions, the variations of the derivatives at the boundary are equal to zero, and the one-time integrals are equal to zero. Integrating the remaining integrals by parts again, we obtain

$$\int_0^{l_x} \int_0^{l_y} dx dy \Delta W(x,y) \Delta \delta W(x,y) =$$

$$= \int_0^{l_y} dy \left[- \int_0^{l_x} dx \frac{\partial}{\partial x} \Delta W(x,y) \frac{\partial}{\partial x} \delta W(x,y) \right] +$$

$$+ \int_0^{l_x} dx \left[- \int_0^{l_y} dy \frac{\partial}{\partial y} \Delta W(x,y) \frac{\partial}{\partial y} \delta W(x,y) \right] =$$

$$= \int_0^{l_y} dy \left[-\Delta W'_x(x,y) \delta W(x,y) \Big|_{x=0}^{x=l_x} + \int_0^{l_x} dx \frac{\partial^2}{\partial x^2} \Delta W(x,y) \delta W(x,y) \right] +$$

$$+ \int_0^{l_x} dx \left[-\Delta W'_y(x,y) \delta W(x,y) \Big|_{y=0}^{y=l_y} + \int_0^{l_y} dy \frac{\partial^2}{\partial y^2} \Delta W(x,y) \delta W(x,y) \right]. \quad (13)$$

Since, in accordance with the boundary conditions

$$W'''_x|_{x=0,l_x} = 0, \quad \frac{\partial^2}{\partial y^2} W'_x|_{x=0,l_x} = 0; \quad W'''_y|_{y=0,l_y} = 0, \quad \frac{\partial^2}{\partial x^2} W'_y|_{y=0,l_y} = 0.$$

Then the one-time integrals in (13) are equal to zero and, thus, we obtain

$$\int_0^{l_x} \int_0^{l_y} dx dy \Delta W(x,y) \Delta \delta W(x,y) = \int_0^{l_y} dy \int_0^{l_x} dx \frac{\partial^2}{\partial x^2} \Delta W(x,y) \delta W(x,y) +$$

$$+\int_0^{l_x} dx \int_0^{l_y} dy \frac{\partial^2}{\partial y^2} \Delta W(x,y)\delta W(x,y) = \int_0^{l_x} dx \int_0^{l_y} dy \Delta^2 W(x,y)\delta W(x,y). \quad (14)$$

Now, for the variation of the functional (10), taking into account (14), we obtain

$$\delta N^\beta[W] = 2(W - F^\mu, \delta W) + 2\beta(\Delta W, \Delta\delta W) = \\ = 2(W - F^\mu, \delta W) + 2\beta(\Delta^2 W, \delta W). \quad (15)$$

Equating the variation to zero and adding boundary conditions (9), we obtain that the extremal of the functional (8) is a solution to the following boundary value problem for the Euler equation

$$\begin{cases} \beta\Delta^2 W + W = F^\mu, \\ W'_x|_{x=0,l_x} = 0, \\ W'_y|_{y=0,l_y} = 0, \\ W'''_x|_{x=0,l_x} = 0, \\ W'''_y|_{y=0,l_y} = 0. \end{cases}$$

We will seek the solution of this boundary value problem in the form of an expansion in the Fourier series

$$W(x,y) = \sum_{n,m=0}^{\infty} \tilde{W}_{nm} \cos\frac{\pi n x}{l_x} \cos\frac{\pi m y}{l_y} \quad (16)$$

in terms of the eigenfunctions of the Laplace operator satisfying the boundary conditions (9)

$$\left\{ \cos\frac{\pi n x}{l_x} \cos\frac{\pi m y}{l_y} \right\}_{n,m=0}^{\infty}. \quad (17)$$

The solution of the boundary value problem for the Euler equation is obtained in the form

$$W^\mu_\beta(x,y) = \sum_{n,m=0}^{\infty} \frac{\tilde{F}^\mu_{nm}}{1+\beta k^4_{nm}} \cos\frac{\pi n x}{l_x} \cos\frac{\pi m y}{l_y}, \quad (18)$$

where, for brevity, the notation is introduced

$$k_{nm} = \pi \left(\frac{n^2}{l_x^2} + \frac{m^2}{l_y^2} \right)^{1/2},$$

and the Fourier coefficients $\tilde{F}^{\mu}_{nm}$ have the form

$$\tilde{F}^{\mu}_{nm} = \frac{4\varepsilon_n\varepsilon_m}{l_x l_y}\int\limits_{\Pi} F^{\mu}(x,y)\cos\frac{\pi n x}{l_x}\cos\frac{\pi m y}{l_y}dxdy, \qquad \varepsilon_n = 1, \quad n \neq 0, \quad \varepsilon_0 = 0.5. \tag{19}$$

It is easy to see that the series (18) converges uniformly on the rectangle Π.

As an approximation to the gradient of the function F^{μ}, we will consider the vector function

$$\nabla_{xy} W^{\mu}_{\beta}(x,y) = \\ = \sum_{n,m=0}^{\infty} \frac{\tilde{F}^{\mu}_{nm}}{1+\beta k^4_{nm}} \left(-\mathbf{i}\frac{\pi n}{l_x}\sin\frac{\pi n x}{l_x}\cos\frac{\pi m y}{l_y} - \mathbf{j}\frac{\pi m}{l_y}\cos\frac{\pi n x}{l_x}\sin\frac{\pi m y}{l_y}\right). \tag{20}$$

The series (20) also converges uniformly on Π. Indeed, applying the Cauchy–Bunyakovsky inequality, in particular, for the x-component of the gradient, we obtain

$$\left|\frac{\partial}{\partial x} W^{\mu}_{\beta}(x,y)\right| \leqslant \\ \leqslant \sum_{n,m=0}^{\infty} \frac{|\tilde{F}^{\mu}_{nm}|}{1+\beta k^4_{nm}}\frac{\pi n}{l_x} \leqslant \sum_{n,m=0}^{\infty} \frac{|\tilde{F}^{\mu}_{nm}| k_{nm}}{1+\beta k^4_{nm}} \leqslant \frac{1}{\beta}\sum_{n,m=0}^{\infty} \frac{|\tilde{F}^{\mu}_{nm}|\sqrt{\varepsilon_n\varepsilon_m}}{k^3_{nm}\sqrt{\varepsilon_n\varepsilon_m}} \leqslant \\ \leqslant \frac{1}{\beta}\left(\frac{4}{l_x l_y}\sum_{n,m=0}^{\infty}\frac{\varepsilon_n\varepsilon_m}{k^6_{nm}}\right)^{\frac{1}{2}} \left(\frac{l_x l_y}{4}\sum_{n,m=0}^{\infty}\frac{(\tilde{F}^{\mu}_{nm})^2}{\varepsilon_n\varepsilon_m}\right)^{\frac{1}{2}} \leqslant \frac{C}{\beta}||F^{\mu}||_{L_2(\Pi)}. \tag{21}$$

A similar estimate can be obtained for the y-component of the gradient. In addition, the uniform convergence of the series (18) is also proved.

Let us now prove the convergence of the series (18) and (20) to F and grad$F$, respectively, as $\mu \to 0$.

Let $F^{+}-$ be an even-periodic continuation of the function F with period $2l_x$ in variable x and period $2l_y$ in variable y from a rectangle Π of the form (5), that is

$$F^{+}(x,y) = F(x,y), \quad (x,y)\in\Pi; \quad F^{+}(-x,y) = F(x,y), \quad (x,y)\in\Pi; \\ F^{+}(x,-y) = F(x,y), \quad (x,y)\in\Pi; \quad F^{+}(-x,-y) = F(x,y), \quad (x,y)\in\Pi; \\ F^{+}(x+2l_x n, y+2l_y m) = F^{+}(x,y), \quad (x,y)\in\mathbb{R}^2, \quad n,m = \pm1, \pm2, ...$$

Theorem 1. *Let* $F^{+} \in C^2(\mathbb{R}^2)$, $M \geqslant \|\Delta F\|_{L_2(\Pi)}$, $\beta = \beta(\mu) = \mu^2/M^2$. *Then*

$$\left\|W^{\mu}_{\beta(\mu)} - F\right\|_{L_2(\Pi)} \leqslant \frac{3}{2}\mu \to 0 \quad as \quad \mu \to 0, \tag{22}$$

$$\left\|\nabla_{xy} W^{\mu}_{\beta(\mu)} - \nabla_{xy} F\right\|_{L_2(\Pi)} \leqslant 2\sqrt{\mu M} \to 0 \quad as \quad \mu \to 0. \tag{23}$$

Proof. Let's introduce a notation for a function of the form (18) for $\mu = 0$

$$W_\beta(x,y) = \sum_{n,m=0}^{\infty} \frac{\tilde{F}_{nm}}{1+\beta k_{nm}^4} \cos\frac{\pi n x}{l_x} \cos\frac{\pi m y}{l_y}. \tag{24}$$

Let us prove the estimate (22) in the assertion of the theorem. Applying the triangle inequality for the norm of the difference $W_\beta^\mu - F$ we obtain

$$\left\|W_\beta^\mu - F\right\|_{L_2(\Pi)} \leqslant \left\|W_\beta^\mu - W_\beta\right\|_{L_2(\Pi)} + \left\|W_\beta - F\right\|_{L_2(\Pi)}. \tag{25}$$

Using the orthogonality of the trigonometric system, for the first norm on the right side (25) we obtain

$$\begin{aligned}\left\|W_{\beta(\mu)}^\mu - W_{\beta(\mu)}\right\|_{L_2(\Pi)}^2 = \\ = \sum_{n,m=0}^{\infty} \frac{\left(\tilde{F}_{nm}^\mu - \tilde{F}_{nm}\right)^2}{\left(1+\beta k_{nm}^4\right)^2} \frac{l_x l_y}{4\varepsilon_n \varepsilon_m} \leqslant \sum_{n,m=0}^{\infty} \frac{\left(\tilde{F}_{nm}^\mu - \tilde{F}_{nm}\right)^2 l_x l_y}{4\varepsilon_n \varepsilon_m} \leqslant \\ \leqslant \left\|F^\mu - F\right\|_{L_2(\Pi)}^2 = \mu^2. \end{aligned} \tag{26}$$

And for the second norm on the right side (25) under the conditions of the theorem, we obtain:

$$\begin{aligned}\left\|W_{\beta(\mu)} - F\right\|_{L_2(\Pi)}^2 = \\ = \sum_{n,m=0}^{\infty} \frac{(\beta k_{nm}^4)^2 \tilde{F}_{nm}^2}{\left(1+\beta k_{nm}^4\right)^2} \frac{l_x l_y}{4\varepsilon_n \varepsilon_m} \leqslant \beta^2 \max_x \left(\frac{x}{1+\beta x^2}\right)^2 \sum_{n,m=0}^{\infty} \frac{k_{nm}^4 \tilde{F}_{nm}^2 l_x l_y}{4\varepsilon_n \varepsilon_m} \leqslant \\ \leqslant \frac{\beta}{4} \left\|\Delta F\right\|_{L_2(\Pi)}^2 \leqslant \frac{\mu^2}{4M^2} M^2 = \frac{\mu^2}{4}. \end{aligned} \tag{27}$$

Here we have used the fact that under the conditions of the theorem

$$\sum_{n,m=0}^{\infty} \frac{k_{nm}^4 \tilde{F}_{nm}^2 l_x l_y}{4\varepsilon_n \varepsilon_m} = \left\|\Delta F\right\|_{L_2(\Pi)}^2 \leqslant M^2, \tag{28}$$

as well as the value of the maximum

$$\max_x \left(\frac{x}{1+\beta x^2}\right) = \frac{1}{2\sqrt{\beta}}.$$

For the difference norm on the left side (25) with $\beta(\mu) = \mu^2/M^2$ from (26) and (27) we obtain

$$\left\|W_{\beta(\mu)}^\mu - F\right\|_{L_2(\Pi)} \leqslant \mu + \frac{\mu}{2} = \frac{3}{2}\mu. \tag{29}$$

We now obtain the estimate (23) by applying the triangle inequality

$$\left\|\nabla_{xy}W_\beta^\mu - \nabla_{xy}F\right\|_{L_2(\Pi)} \leqslant$$
$$\leqslant \left\|\nabla_{xy}W_\beta^\mu - \nabla_{xy}W_\beta\right\|_{L_2(\Pi)} + \left\|\nabla_{xy}W_\beta - \nabla_{xy}F\right\|_{L_2(\Pi)}. \quad (30)$$

Estimate the first difference in on the right side (30):

$$\left\|\nabla_{xy}W_\beta^\mu - \nabla_{xy}W_\beta\right\|^2_{L_2(\Pi)} = \int\limits_\Pi \left| -\mathbf{i}\sum_{n,m=0}^{\infty} \frac{\tilde F_{nm}^\mu - \tilde F_{nm}}{1+\beta k_{nm}^4}\frac{\pi n}{l_x}\sin\frac{\pi n x}{l_x}\cos\frac{\pi m y}{l_y} - \right.$$
$$\left. -\mathbf{j}\sum_{n,m=0}^{\infty} \frac{\tilde F_{nm}^\mu - \tilde F_{nm}}{1+\beta k_{nm}^4}\frac{\pi m}{l_y}\sin\frac{\pi m y}{l_y}\cos\frac{\pi n x}{l_x}\right|^2 dxdy =$$
$$= \int\limits_\Pi \left|\sum_{n,m=0}^{\infty} \frac{\tilde F_{nm}^\mu - \tilde F_{nm}}{1+\beta k_{nm}^4}\frac{\pi n}{l_x}\sin\frac{\pi n x}{l_x}\cos\frac{\pi m y}{l_y}\right|^2 dxdy +$$
$$+ \int\limits_\Pi \left|\sum_{n,m=0}^{\infty} \frac{\tilde F_{nm}^\mu - \tilde F_{nm}}{1+\beta k_{nm}^4}\frac{\pi m}{l_y}\sin\frac{\pi m y}{l_y}\cos\frac{\pi n x}{l_x}\right|^2 dxdy. \quad (31)$$

Using the orthogonality of the trigonometric system, we obtain:

$$\left\|\nabla_{xy}W_\beta^\mu - \nabla_{xy}W_\beta\right\|^2_{L_2(\Pi)} = \sum_{n,m=0}^{\infty} \frac{\left(\tilde F_{nm}^\mu - \tilde F_{nm}\right)^2}{\left(1+\beta k_{nm}^4\right)^2}\left(\frac{\pi n}{l_x}\right)^2 \frac{l_x l_y}{4\varepsilon_n\varepsilon_m} +$$
$$+ \sum_{n,m=0}^{\infty} \frac{\left(\tilde F_{nm}^\mu - \tilde F_{nm}\right)^2}{\left(1+\beta k_{nm}^4\right)^2}\left(\frac{\pi m}{l_y}\right)^2 \frac{l_x l_y}{4\varepsilon_n\varepsilon_m} = \frac{l_x l_y}{4}\sum_{n,m=0}^{\infty} \frac{\left(\tilde F_{nm}^\mu - \tilde F_{nm}\right)^2 k_{nm}^2}{\varepsilon_n\varepsilon_m\left(1+\beta k_{nm}^4\right)^2} \leqslant$$
$$\leqslant \max_x\left(\frac{x}{1+\beta x^4}\right)^2 \sum_{n,m=0}^{\infty} \frac{\left(\tilde F_{nm}^\mu - \tilde F_{nm}\right)^2 l_x l_y}{4\varepsilon_n\varepsilon_m} = \frac{1}{\sqrt{\beta}}\left\|F^\mu - F\right\|^2_{L_2(\Pi)}. \quad (32)$$

Here we have used the estimate for the maximum

$$\max_x\left(\frac{x}{1+\beta x^4}\right) = \frac{3^{3/4}}{4}\beta^{-1/4} \leqslant \beta^{-1/4}.$$

Extracting the root at (32), we obtain for the first difference at (30):

$$\left\|\nabla_{xy}W_\beta^\mu - \nabla_{xy}W_\beta\right\|_{L_2(\Pi)} \leqslant \frac{1}{\sqrt[4]{\beta}}\left\|F^\mu - F\right\|_{L_2(\Pi)} = \frac{\mu}{\sqrt[4]{\beta}}. \quad (33)$$

Similarly, to evaluate the second difference in (30), using (24), we obtain:

$$\left\|\nabla_{xy}W_\beta - \nabla_{xy}F\right\|^2_{L_2(\Pi)} = \beta^2\frac{l_x l_y}{4}\sum_{n,m=0}^{\infty}\frac{\tilde{F}^2_{nm}\left[k^4_{nm}\right]^2 k^2_{nm}}{\varepsilon_n\varepsilon_m\left(1+\beta k^4_{nm}\right)^2} \leqslant$$

$$\leqslant \beta^2\max_x\left(\frac{x^3}{1+\beta x^4}\right)^2\sum_{n,m=0}^{\infty}\frac{(\tilde{F}_{nm}k^2_{nm})^2 l_x l_y}{4\varepsilon_n\varepsilon_m} = \sqrt{\beta}\left\|\Delta F\right\|^2 = \sqrt{\beta}M^2. \quad (34)$$

Here we have used the estimate for the maximum

$$\max_x\left(\frac{x^3}{1+\beta x^4}\right) = \frac{3^{3/4}}{4}\beta^{-3/4} \leqslant \beta^{-3/4},$$

and also by the fact that under the conditions of the theorem

$$\Delta F = \sum_{n,m=0}^{\infty}\tilde{F}_{nm}k^2_{nm}\cos\frac{\pi n x}{l_x}\cos\frac{\pi m y}{l_y}.$$

Therefore, the second norm on the right side (30) after taking the square root in (34) evaluates to

$$\left\|\nabla_{xy}W_\beta - \nabla_{xy}F\right\|_{L_2(\Pi)} \leqslant \sqrt[4]{\beta}M. \quad (35)$$

Thus, using the estimates (34), (35) and the conditions of the theorem on the function $\beta(\mu)$, from (30) we obtain an error estimate in calculating the gradient of the function F:

$$\left\|\nabla_{xy}W^\mu_{\beta(\mu)} - \nabla_{xy}F\right\|_{L_2(\Pi)} \leqslant \frac{\mu}{\sqrt[4]{\beta}} + \sqrt[4]{\beta}M \leqslant 2\sqrt{\mu M} \to 0 \quad \text{as} \quad \mu \to 0. \quad (36)$$

Note that for $\beta(\mu) = \mu^2/M^2$, the expression on the right represents the minimum by the parameter β.

The theorem is proved. □

Based on this theorem, we can use the formula for the approximate gradient to construct an approximate normal to the surface S by the formula (6)

$$\mathbf{n}^\mu_1 = \nabla_{xy}W^\mu_{\beta(\mu)} - \mathbf{k}. \quad (37)$$

then from (37) and (36) follows an estimate of the deviation of the approximate normal $\mathbf{n}^\mu_1$ from the exact:

$$\left\|\mathbf{n}^\mu_1 - \mathbf{n}_1\right\|_{L_2(\Pi)} = \left\|\nabla_{xy}W^\mu_\beta - \nabla_{xy}F\right\|_{L_2(\Pi)} \leqslant 2\sqrt{\mu M}.$$

The surface defined by the equation $z = W^\mu_{\beta(\mu)}(x,y)$, where $W^\mu_{\beta(\mu)}$ has the form (18), denote

$$S^\mu = \left\{(x,y,z) : 0 < x < l_x,\, 0 < y < l_y,\, z = W^\mu_{\beta(\mu)}(x,y)\right\}. \quad (38)$$

Since the series (18) converges uniformly, the surface S^μ is given by a continuous function.

When solving various problems of mathematical physics that use surface integrals and a normal derivative on a surface given approximately by the condition (7), an approximately given surface $z = F^\mu(x, y)$ can be replaced by the surface S^μ, and the normal to the surface can be calculated according to the formula (37).

4. Application of the problem of calculating the normal to the inverse problem of thermography

Calculation of the normal to the surface may be necessary, in particular, when solving the inverse problem of thermography. In this case, we consider the problem of correcting the thermogram f, which is a digitized temperature distribution on the surface of the investigated heat-conducting body containing heat sources. The image of body sources on a thermogram is, as a rule, distorted due to the process of heat conduction, heat transfer, and the relative remoteness of heat sources from the body surface. In order to refine the image in a cylindrical area of rectangular cross section

$$D(F, H) = \{(x, y, z) : 0 < x < l_x,\ 0 < y < l_y,\ F(x, y) < z < H\}. \tag{39}$$

a boundary value problem for the Laplace equation is considered (we assume that the support of the heat source density function ρ is located in the region $z > H$)

$$\begin{cases} \Delta u(M) = 0, \quad M \in D(F, H), \\ u\big|_S = f, \\ \dfrac{\partial u}{\partial n}\Big|_S = h(U_0 - f)\Big|_S, \\ u|_{\Gamma_H} = 0. \end{cases} \tag{40}$$

The set of side faces of $D(F, H)$ is denoted as Γ_H.

Note that in the problem (40) on the surface S of the form (3), the Cauchy conditions are specified, that is, the boundary values f of the desired function u and the values of its normal derivative are given, so the problem (40) has a unique solution. The boundary $z = H$ of the domain $D(F, H)$ is free and thus the problem (40) is not robust against data errors, i.e. ill-posed.

The function $u|_{z=H}$ will be considered as an adjusted thermogram. Since the plane $z = H$ is located closer to the density carrier ρ than the surface S from which the original thermogram is taken, it should be expected that the corrected thermogram more accurately conveys information about the distribution of heat sources than the original thermogram.

We will assume that the function f in the problem (40) is given with an error, that is, instead of f, the function f^δ is given, such that

$$\left\|f^\delta - f\right\|_{L_2(\Pi)} \leqslant \delta. \tag{41}$$

In [12], an approximate solution to an ill-posed problem (40) is constructed as

$$u_\alpha^\delta(M) = v_\alpha^\delta(M) + \Phi^\delta(M), \quad M \in D(F,H), \tag{42}$$

where the function

$$\Phi^\delta(M) = \int\limits_\Pi \Big[h(U_0 - f^\delta(x_P,y_P))\varphi(M,P)\big|_{P\in S} n_1(x_P,y_P) - \\ - f^\delta(x_P,y_P)(\mathbf{n}_1, \nabla_P\varphi(M,P))\big|_{P\in S}\Big]dx_P dy_P \tag{43}$$

is calculated using the problem data (40) and the Dirichlet problem source function

$$\varphi(M,P) = \\ = \frac{2}{l_x l_y}\sum_{n,m=1}^{\infty} \frac{e^{-k_{nm}|z_M - z_P|}}{k_{nm}} \times \sin\frac{\pi n x_M}{l_x}\sin\frac{\pi m y_M}{l_y}\sin\frac{\pi n x_P}{l_x}\sin\frac{\pi m y_P}{l_y}, \tag{44}$$

$$k_{nm} = \pi\left(\frac{n^2}{l_x^2} + \frac{m^2}{l_y^2}\right)^{1/2}$$

in the infinite cylinder

$$D^\infty = \{(x,y,z) : 0 < x < l_x,\, 0 < y < l_y,\, -\infty < z < \infty\} \subset \mathbb{R}^3.$$

The function v_α^δ, which is an approximation to the density potential ρ, in [12] is obtained using the Tikhonov regularization method [1]

$$v_\alpha^\delta(M) = \\ = -\sum_{n,m=1}^{\infty} \frac{\tilde{\Phi}_{nm}^\delta(a)\exp\{k_{nm}(z_M - a)\}}{1 + \alpha\exp\{2k_{nm}(H-a)\}}\sin\frac{\pi n x_M}{l_x}\sin\frac{\pi m y_M}{l_y}, \quad \alpha > 0, \tag{45}$$

$\tilde{\Phi}_{nm}^\delta(a)$ are Fourier coefficients of the function $\Phi^\delta(M)$ of the form (43)

$$\tilde{\Phi}_{nm}^\delta(a) = \frac{4}{l_x l_y}\int\limits_\Pi \Phi^\delta(x,y,a)\sin\frac{\pi n x}{l_x}\sin\frac{\pi m y}{l_y}dxdy. \tag{46}$$

As follows from the formula (43) when calculating the value of Φ, the normal to the surface is used. Estimates of the error in calculating the function Φ and the approximate solution u that arise when replacing the exact normal $\mathbf{n}_1$ with an approximate normal are obtained in [13].

5. Conclusion and discussion

Formulas (37), (20) for approximate calculation of the normal to an approximately given surface can be used in the calculation of surface integrals

and potentials of a simple and double layer and in other problems [14] using the normal to the surface. For numerical summation of Fourier series (45) and calculation of Fourier coefficients (46) algorithms for summing discrete Hamming series [15, 16] can be used. Discretization of formulas (45), (46) can be done in accordance with [17].

References

[1] A. N. Tikhonov and V. J. Arsenin, *Methods for solving ill-posed problems [Metody resheniya nekorrektnyh zadach]*. Moscow: Nauka, 1979, in Russian.

[2] T. F. Dolgopolova and V. K. Ivanov, "On numerical differentiation," *USSR Computational Mathematics and Mathematical Physics*, vol. 6, no. 3, pp. 223–232, 1966. DOI: 10.1016/0041-5553(66)90145-5.

[3] V. V. Vasin, "The stable evaluation of a derivative in space $C(-\infty, \infty)$," *USSR Computational Mathematics and Mathematical Physics*, vol. 13, no. 6, pp. 16–24, 1973, english. DOI: 10.1016/0041-5553(73)90002-5.

[4] R. S. Anderssen and P. Bloomfield, "Numerical differentiation procedures for non-exact data," *Numerische Mathematik*, vol. 22, pp. 157–182, 1974. DOI: 10.1007/BF01436965.

[5] C. W. Groetsch, "Optimal order of accuracy in Vasin's method for differentiation of noisy functions," *Journal of Optimization Theory and Applications*, vol. 74, pp. 373–378, 1992. DOI: 10.1007/BF00940901.

[6] M. Hanke and O. Scherzer, "Inverse problems light: Numerical differentiation," *American Mathematical Monthly*, vol. 108, no. 6, pp. 512–521, 2001, english. DOI: 10.1080/00029890.2001.11919778.

[7] S. Ahn, U. J. Choi, and A. G. Ramm, "A scheme for stable numerical differentiation," *Journal of Computational and Applied Mathematics*, vol. 186, no. 6, pp. 325–334, 2006, english. DOI: 10.1016/j.cam.2005.02.002.

[8] Z. Meng, Z. Zhao, D. Mei, and Y. Zhou, "Numerical differentiation for two-dimensional functions by a Fourier extension method," *Inverse Problems in Science and Engineering*, vol. 28, no. 1, pp. 126–143, 2020, english. DOI: 10.1080/17415977.2019.1661410.

[9] E. V. Semenova, S. G. Solodky, and S. A. Stasyuk, "Application of Fourier truncation method to numerical differentiation for bivariate functions," *Computational Methods in Applied Mathematics*, vol. 22, no. 2, pp. 477–491, 2022, english. DOI: 10.1515/cmam-2020-0138.

[10] V. A. Morozov, "On a stable method for computing the values of unbounded operators [Ob odnom ustoychivom metode vychisleniya znacheniy neogranichennykh operatorov]," *Dokladi AN SSSR*, vol. 185, no. 2, pp. 267–270, 1969, in Russian.

[11] E. B. Laneev and M. N. Muratov, "On the stable solution of a mixed boundary value problem for the Laplace equation with an approximately given boundary [Ob ustoychivom reshenii smeshannoy krayevoy zadachi dlya uravneniya Laplasa s priblizhenno zadannoy granitsey]," *Vestnik RUDN. Matematika*, vol. 9, no. 1, pp. 102–111, 2002, in Russian.

[12] E. B. Laneev, N. Y. Chernikova, and O. Baaj, "Application of the minimum principle of a Tikhonov smoothing functional in the problem of processing thermographic data," *Advances in Systems Science and Applications*, no. 1, pp. 139–149, 2021. DOI: 10.25728/assa.2021.21.1.1055.

[13] O. Baaj, N. Y. Chernikova, and E. B. Laneev, "Correction of thermographic images based on the minimization method of Tikhonov functional," *Yugoslav Journal of Operations Research*, vol. 32, no. 3, pp. 407–424, 2022. DOI: 10.2298/YJOR211015026B.

[14] E. B. Laneev and E. Y. Ponomarenko, "On a linear inverse potential problem with approximate data on the potential field on an approximately given surface," *Eurasian mathematical journal*, vol. 14, no. 1, pp. 57–70, 2023. DOI: 10.32523/2077-9879-2023-14-1-55-70.

[15] R. W. Hamming, *Numerical methods for scientists and engineers*. New York: McGraw-Hill Book Company, 1962.

[16] E. B. Laneev and O. Baaj, "On a modification of the Hamming method for summing discrete Fourier series and its application to solve the problem of correction of thermographic images," *Discrete and Continuous Models and Applied Computational Science*, vol. 30, no. 4, pp. 342–356, 2022. DOI: 10.22363/2658-4670-2022-30-4-342-356.

[17] E. B. Laneev, M. N. Mouratov, and E. P. Zhidkov, "Discretization and its proof for numerical solution of a Cauchy problem for Laplace equation with inaccurately given Cauchy conditions on an inaccurately defined arbitrary surface," *Physics of Particles and Nuclei Letters*, vol. 5, no. 3, pp. 164–167, 2002. DOI: 10.1134/S1547477108030059.

For citation:

E. B. Laneev, O. Baaj, On a stable calculation of the normal to a surface given approximately, Discrete and Continuous Models and Applied Computational Science 31 (3) (2023) 228–241. DOI: 10.22363/2658-4670-2023-31-3-228-241.

Information about the authors:

Laneev, Evgeniy B. — Doctor of Physical and Mathematical Sciences, professor of Mathematical Department of Peoples' Friendship University of Russia named after Patrice Lumumba (RUDN University) (e-mail: elaneev@yandex.ru, phone: +7(903)1333622, ORCID: https://orcid.org/0000-0002-4255-9393)

Baaj, Obaida — Post-Graduate Student of Mathematical Department of Peoples' Friendship University of Russia named after Patrice Lumumba (RUDN University) (e-mail: 1042175025@rudn.ru, phone: +7(916)6890863, ORCID: https://orcid.org/0000-0003-4813-7981)

УДК 519.6
PACS 07.05.Tp, 02.60.Pn, 02.70.Bf
DOI: 10.22363/2658-4670-2023-31-3-228-241
EDN: KNQAEY

Об устойчивом вычислении нормали к поверхности, заданной приближённо

Е. Б. Ланеев, Обаида Бааж

Российский университет дружбы народов,
ул. Миклухо-Маклая, д. 6, Москва, 117198, Россия

Аннотация. В работе предлагается устойчивый метод построения нормали к поверхности, заданной приближённо. Нормаль вычисляется как градиент функции в уравнении поверхности. Как известно, задача вычисления производной является некорректно поставленной. В работе принят подход к решению этой задачи как к задаче вычисления значений неограниченного оператора. Для построения её устойчивого решения используется принцип минимума сглаживающего функционала в формулировке Морозова. Нормаль получена в виде ряда Фурье в разложении по собственным функциям оператора Лапласа в прямоугольнике с краевыми условиями второго рода. В стабилизаторе функционала используется лапласиан, что позволяет получить нормаль в виде ряда Фурье, равномерно сходящегося к точному вектору нормали при стремлении к нулю погрешности в задании поверхности. Полученный приближенный вектор нормали может использоваться при решении различных задач математической физики, использующих поверхностные интегралы, нормальные производные, потенциалы простого и двойного слоя.

Ключевые слова: некорректная задача, устойчивое вычисление производной, метод регуляризации, дискретный ряд Фурье

Discrete & Continuous Models & Applied Computational Science
ISSN 2658-7149 (online), 2658-4670 (print)
2023, 31 (3) 242–246
http://journals.rudn.ru/miph

Research article

UDC 531.5:531-9
PACS 04.50.Kd, 04.30.-w, 02.40.Ky
DOI: 10.22363/2658-4670-2023-31-3-242-246
EDN: XYOZDS

Hodge–de Rham Laplacian and geometric criteria for gravitational waves

Olga V. Babourova[1], **Boris N. Frolov**[2]

[1] *Moscow Automobile and Road Construction State Technical University (MADI), 64, Leningradsky pr., Moscow, 125319, Russian Federation*
[2] *Institute of Physics, Technology and Information Systems, Moscow Pedagogical State University (MSPU), 29/7, M. Pirogovskaya str., Moscow, 119435, Russian Federation*

(received: July 7, 2023; revised: July 25, 2023; accepted: September 8, 2023)

Abstract. The curvature tensor $\hat{R}$ of a manifold is called harmonic, if it obeys the condition $\Delta^{(\mathrm{HR})}\hat{R} = 0$, where $\Delta^{(\mathrm{HR})} = DD^* + D^*D$ is the Hodge–de Rham Laplacian. It is proved that all solutions of the Einstein equations in vacuum, as well as all solutions of the Einstein–Cartan theory in vacuum have a harmonic curvature. The statement that only solutions of Einstein's equations of type N (describing gravitational radiation) are harmonic is refuted.

Key words and phrases: Hodge–de Rham Laplacian, harmonic curvature tensor, harmonic solutions in vacuum of Einstein equation and Einstein–Cartan theory equations

1. Introduction. Harmonic curvature tensor

In non-Euclidean spaces, in the formalism of differential forms, an external covariant differential D is defined, as well as an external covariant codifferential D^*, whose action on the p-form ω is determined by the rule:

$$D^*\omega = (-1)^p *^{-1} D * \omega,$$

where $*$ is the Hodge dualization operator mapping differential forms onto polyvectors and vice versa. The inverse operator $*^{-1}$ is determined by the rule: $*^{-1} = (-1)^{q(n-q)+s}*$, where n is the dimension of the manifold, s is the sign of the determinant of the metric, and q is the degree of the form on which the operator $*^{-1}$ acts. As a result, in the definition of D^* the operator $*^{-1}$ acts on the $D * \omega$ form of the degree $q = n - p + 1$. As a consequence, the action of the codifferential D^* can be represented in an equivalent form

as: $D^*\omega = (-1)^{np+n+1+s} * D * \omega$, which for a 4-dimensional pseudo-Euclidean space and a form ω of even degree gives $D^*\omega = *D * \omega$ [1, 2].

A differential form is said to be *harmonic* if the action of the Hodge–de Rham Laplacian $\Delta^{(\mathrm{HR})} = DD^* + D^*D$ on it is identically equal to zero. In particular, if the curvature 2-form $\hat{R}$ satisfies the condition $\Delta^{(\mathrm{HR})}\hat{R} = 0$, then the corresponding curvature tensor is said to be *harmonic* [3, 4]. In Riemann space, this condition in coordinates is fulfilled if the equation $\nabla_\lambda R^\lambda_{\sigma\mu\nu} = 0$ is satisfied.

2. Hodge–de Rham Laplacian in gauge field theories

The Hodge–de Rham Laplacian arises in geometrized gauge theories. For example, a similar operator arises in the geometric interpretation of the Yang–Mills theory as a theory of fiber bundle, where the exterior differential d and co-differential δ are defined, as well as the operator $\Delta = d\delta + \delta d$, which in this case is called the Laplace-Beltrami Laplacian. This operator plays an essential role in the theory, since the Yang–Mills gauge field equations follow from the condition $\Delta = 0$. In this geometric interpretation the comparison of the potentials of the Yang–Mills gauge field and the linear connection of the fiber bundle is important [5].

In the geometric interpretation of the gravitational field in the Poincaré-gauge theory of gravity (PGTG) as the theory of an affine fibred space arising as a consequence of the localization of the Poincaré group, the Hodge–de Rham Laplacian $\Delta^{(\mathrm{HR})} = DD^* + D^*D$ also arises.

3. Hodge–de Rham Laplacian and geometric criterion of gravitational radiation

Earlier in the literature, when discussing various geometric criteria of gravitational radiation, one could come across the statement that those and only those Einstein spaces of type N describing gravitational radiation are harmonic (that is, for which the equality $\Delta^{(\mathrm{HR})}\hat{R} = 0$ is satisfied). The Einstein space is understood as the space in which the Einstein equation in vacuum $R_{\alpha\beta} = \Lambda g_{\alpha\beta}$ is satisfied.

Let us prove that this statement is erroneous, although it is given in the well-known monograph on gravitational waves [6].

4. On the property of harmonic solutions of the general theory of relativity and Poincaré-gauge theory of gravity

Let us find out what role the Hodge–de Rham Laplacian plays in the general theory of relativity and the Poincaré-gauge theory of gravity.

In authors' paper [7] the detailed calculation of the result of the action of the Hodge–de Rham Laplacian on the curvature 2-form $\hat{R}$ of the Riemann space of general relativity is given.

The intermediate result is:

$$\Delta^{(\mathrm{HR})}\hat{R} = (1/2)\left(R^{\lambda}_{\sigma\mu\nu;\rho}{}^{;\rho} + R^{\lambda\ \ \rho}_{\sigma\mu\ [;\rho;\nu]} - R^{\lambda\ \ \rho}_{\sigma\nu\ [;\rho;\mu]}\right)\bar{e}_{\lambda}\otimes\bar{e}^{\sigma}\otimes\theta^{\mu}\wedge\theta^{\nu},$$

where $\bar{e}_{\lambda}$ is the coordinate basis of vectors; θ^{μ} are the basic 1-forms, $\wedge$ is the external multiplication; the symbol "semicolon" means covariant differentiation of the components of the curvature tensor.

We substitute into this equality the identity $R^{\lambda}_{\sigma\mu\nu;\rho}{}^{;\rho} = R^{\lambda\ \ \rho}_{\sigma\mu\ ;\nu;\rho} - R^{\lambda\ \ \rho}_{\sigma\nu\ ;\mu;\rho}$ obtained by the Bianchi identity contraction. As a result, we get:

$$\Delta^{(\mathrm{HR})}\hat{R} = \left(R_{\lambda\sigma\mu}{}^{\rho}_{;\rho}\right)_{;\nu}\theta^{\lambda}\wedge\theta^{\sigma}\otimes\theta^{\mu}\wedge\theta^{\nu}.$$

Based on this result, the statement was proved in [7]:

All solutions of Einstein's equation $R_{\alpha\beta} = \Lambda g_{\alpha\beta}$ in vacuum are harmonic.

The proof is based on the equality $R_{\lambda\sigma\mu}{}^{\rho}_{;\rho} = 2R_{\mu[\lambda;\sigma]} = 0$, which is a consequence of the Bianchi identity and the Einstein equation in vacuum. The right side of this equality is called the Codazzi equation. Note that this assertion was stated in [8] (without calculations) and is also known to geometers [4].

The authors have calculated the result of the action of the Hodge–de Rham Laplacian on the curvature 2-form $\overset{C}{\hat{R}}$ in the PGTG in spaces with torsion:

$$\Delta^{(\mathrm{HR})}\ \overset{C}{\hat{R}} = \left[\left(\nabla_{\mu}\delta^{\kappa}_{\nu} + 1/2T^{\kappa}_{\mu\nu}\right)\left(\nabla_{\mu}\delta^{\alpha}_{\kappa} + 1/2T^{\alpha\beta}_{\kappa} + \delta^{\alpha}_{\kappa}T^{\beta}\right)R^{\lambda}_{\sigma\alpha\beta}\right]\bar{e}_{\lambda}\otimes\bar{e}^{\sigma}\otimes\theta^{\mu}\wedge\theta^{\nu}.$$

Here, $T^{\kappa}_{\mu\nu}$ is the torsion tensor, T^{κ} is its trace and ∇_{μ} is the symbol of covariant differentiation.

If we confine ourselves to a special case of the Riemann–Cartan space, then the consequence of this expression is the statement:

The solutions of the equations of the gravitational field of the Einstein–Cartan theory in vacuum are harmonic.

The proof is based on the fact that in the Einstein–Cartan theory one of the equations of the gravitational field in vacuum is $T^{\kappa}_{[\alpha\beta]} + 2\delta^{\kappa}_{[\alpha}T_{\beta]} = 0$, and then on the use of the proved statement for general relativity.

5. Conclusion

Thus, it has been shown that both the general theory of relativity and the Poincaré-gauge theory of gravity (in the particular case of the Einstein–Cartan theory) have a property similar to the Yang–Mills and Maxwell electromagnetism theories, namely, the solutions of the field equations of these theories in vacuum are harmonic, what demonstrates the generality of the gauge theory of gravity with other gauge theories.

It is also shown that the assertion existing in the literature that the equality $\Delta^{(\mathrm{HR})}\hat{R} = 0$ holds only for solutions of the Einstein equation in vacuum of type N, and therefore can serve as a criterion for the presence of gravitational radiation, is an erroneous assertion, although it is indicated in the well-known monograph by V. D. Zakharov [6].

References

[1] G. de Rham, *Differentiable manifolds: forms, currents, harmonic forms*. Berlin, Heidelberg, New York, Tokyo: Springer-Verlag, 2011, 180 pp.

[2] M. O. Katanaev, "Geometric methods in mathematical physics," in Russian. arXiv: 1311.0733v3 [math-ph].

[3] A. L. Besse, *Einstein manifolds*. Berlin, Heidelberg: Springer-Verlag, 1987.

[4] J.-P. Bourguignon, "Global riemannian geometry," in T. J. Willmore and N. J. Hitchin, Eds. New York: Ellis Horwood Lim., 1984, ch. Metric with harmonic curvature.

[5] D. A. Popov, "To the theory of the Yang–Mills fields," *Theoretical and mathematical physics*, vol. 24, no. 3, pp. 347–356, 1975, in Rusian.

[6] V. D. Zakharov, *Gravitational waves in Einstein's theory of gravitation*. Moscow: Nauka, 1972, 200 pp., in Rusian.

[7] O. V. Babourova and B. N. Frolov, "On a harmonic property of the Einstein manifold curvature," 1995. arXiv: gr-qc/9503045v1.

[8] D. A. Popov and L. I. Dajhin, "Einstein spaces and Yang–Mills fields," *Reports of the USSR Academy of Sciences [Doklady Akademii nauk SSSR]*, vol. 225, no. 4, pp. 790–793, 1975.

For citation:

O. V. Babourova, B. N. Frolov, Hodge–de Rham Laplacian and geometric criteria for gravitational waves, Discrete and Continuous Models and Applied Computational Science 31 (3) (2023) 242–246. DOI: 10.22363/2658-4670-2023-31-3-242-246.

Information about the authors:

Babourova, Olga V. — Professor, Doctor of Sciences in Physics and Mathematics, Professor at Department Physics, Moscow Automobile and Road Construction State Technical University (MADI) (e-mail: ovbaburova@madi.ru, phone: +7(499)155-03-90, ORCID: https://orcid.org/0000-0002-2527-5268)

Frolov, Boris N. — Professor, Doctor of Sciences in Physics and Mathematics, Professor at Department of Theoretical Physics, Institute of Physics, Technology and Information Systems, Moscow Pedagogical State University (MSPU) (e-mail: bn.frolov@mpgu.su, phone: +7(499)255-70-04, ORCID: https://orcid.org/0000-0002-8899-1894)

УДК 531.5:531-9
PACS 04.50.Kd, 04.30.-w, 02.40.Ky
DOI: 10.22363/2658-4670-2023-31-3-242-246
EDN: XYOZDS

Лапласиан Ходжа–де Рама и геометрический критерий для гравитационных волн

О. В. Бабурова[1], **Б. Н. Фролов**[2]

[1] *Московский автодорожный государственный технический университет, Ленинградский пр-т, д. 64, Москва, 125319, Россия*
[2] *Институт физики, технологии и информационных систем, Московский педагогический государственный университет, М. Пироговская ул., д. 29/7, Москва, 119435, Россия*

Аннотация. Тензор кривизны $\hat{R}$ многообразия называется гармоничным, если он подчиняется условию $\Delta^{(\mathrm{HR})}\hat{R} = 0$, где $\Delta^{(\mathrm{HR})} = DD^* + D^*D$ — лапласиан Ходжа-де Рама. Доказывается, что все решения уравнений Эйнштейна в пустоте, а также все решения теории Эйнштейна–Картана в пустоте обладают гармоничной кривизной. Опровергается утверждение о том, что гармоничными являются только решения уравнений Эйнштейна типа N, описывающее гравитационное излучение.

Ключевые слова: Лапласиан Ходжа–де Рама, гармоничный тензор кривизны, гармоничные решения в пустоте уравнений Эйнштейна и уравнений теории Эйнштейна–Картана

Discrete & Continuous Models
& Applied Computational Science
ISSN 2658-7149 (online), 2658-4670 (print)

2023, 31 (3) 247–259
http://journals.rudn.ru/miph

Research article

UDC 514.74:530.145
PACS 03.65.Fd, 03.65.Ca, 02.10.Ud,
DOI: 10.22363/2658-4670-2023-31-3-247-259
EDN: KRDBEG

Hamiltonian simulation in the Pauli basis of multi-qubit clusters for condensed matter physics

Eduardo L. André[1, 2], **Alexander N. Tsirulev**[2]

[1] *Faculty of Sciences, Agostinho Neto University, 7, Avenida 4 de Fevereiro, Luanda, Angola*
[2] *Faculty of Mathematics, Tver State University, 35, Sadovyi, Tver, 170002, Russian Federation*

(received: August 16, 2023; revised: August 25, 2023; accepted: September 8, 2023)

Abstract. We propose an efficient method for Hamiltonian simulation of multi-qubit quantum systems with special types of interaction. In our approach, the Hamiltonian of a n-qubit system should be represented as a linear combination of the standard Pauli basis operators, and then decomposed into a sum of partial Hamiltonians, which are, in general, not Pauli operators and satisfy some anticommutation relations. For three types of Hamiltonians, which are invariant with respect to permutations of qubits, the effectiveness of the main algorithm in the three-qubit cluster model is shown by calculating the operator exponentials for these Hamiltonians in an explicit analytical form. We also calculate the density operator, partition function, entropy, and free energy of the cluster weakly coupled to a thermal environment. In our model, the cluster is in the Gibbs state in the temperature interval $0.1-2$K, which corresponds to the operating range of modern quantum processors. It follows from our analysis that the thermodynamic properties of such systems strongly depend on the type of internal interaction of qubits in the cluster.

Key words and phrases: Hamiltonian simulation, cluster of qubits, operator exponential, thermal environment, Gibbs state, thermodynamic properties

1. Introduction

In recent decades, effective mathematical methods and computational algorithms have been developed to simulate the dynamics of quantum systems and their thermodynamic properties on classical computers. It is believed that classical modeling of quantum systems, at least in quantum computation and chemical physics [1, 2], is potentially the shortest path to substantive quantum algorithms. In quantum information and condensed matter physics, the Hamiltonian simulation is one of the most important problems [3–5]. This problem can be mathematically formulated as the task of computing, exactly

or approximately, the operator exponential $\exp\left(\tau\hat{H}\right)$ for a Hamiltonian of the form $\hat{H} = \sum \hat{H}_k$, where each summand is assumed to be a Hermitian operator [6, 7]. Usually the simulating Hamiltonian has a simpler form in comparison with the Hamiltonian of a real quantum system, but they both have the same specific features; in particular, their spectra should be close to each other.

In this paper we propose a method for computing the operator exponentials based on the decomposition of a simulating Hamiltonian into a linear combination of n-qubit Pauli operators to reduce the complexity of the computations. The method is suitable for Hamiltonians of a certain type, which, nevertheless, represent a wide class of quantum systems in condensed matter physics. Note that we will understand the problem of Hamiltonian simulation in a wide sense. Namely, if the parameter τ is purely imaginary, say $\tau = -it$, then the operator exponential describes the unitary time evolution of a closed quantum system. On the other hand, the exponential $\exp\left(-\beta\hat{H}\right)/Z$ is the density operator of a quantum subsystem weakly interacting with a thermal environment having the inverse temperature β. We will consider only time-independent Hamiltonians.

The paper is organized as follows. Sec. 2 contains some mathematical preliminaries, in particular necessary definitions and properties of the Pauli basis. Sec. 3 is devoted to the description of our method and the corresponding algorithm. In Sec. 4 we consider a cluster consisting of three qubits, three model Hamiltonians for different types of interaction, and compute the corresponding exponentials and spectra. Sec. 5 deals with the same cluster interacting with a thermal environment. In the last two sections, our goal is twofold: first, we want to demonstrate the proposed method with a specific example (which admits fully analytical calculations), and second, to present a prototype of some realistic models for clusters that include a three-qubit interaction.

Throughout the paper, we use the natural system of units with $c = 1$, $\hbar = 1$, and $k_B = 1$, so that energy and temperature are measured in units of inverse length.

2. Pauli basis

Let $\mathcal{H}$ be a one-qubit Hilbert space and $\mathcal{H}_n = \mathcal{H}^{\otimes n}$ be the corresponding 2^n-dimensional Hilbert space for a quantum system of n distinguishable qubits. Let $L(\mathcal{H}_n) = \mathcal{H}_n \otimes \mathcal{H}_n^\dagger$ be the space of linear operators acting on $\mathcal{H}_n$ and $\mathcal{H}_n^\dagger$ by the left and right contractions respectively. It is obvious that $L(\mathcal{H}_n)$ is a Hilbert space with respect to the Hilbert-Schmidt inner product, $\langle \hat{A}, \hat{B}\rangle = \operatorname{tr}(\hat{A}^\dagger \hat{B})$, $\hat{A}, \hat{B} \in L(\mathcal{H}_n)$, and obviously $\dim_{\mathbb{C}} L(\mathcal{H}_n) = 4^n$. The identity operator, $\hat{\sigma}_0 = |0\rangle\langle 0| + |1\rangle\langle 1|$, and the three Pauli operators

$$\hat{\sigma}_1 = |0\rangle\langle 1| + |1\rangle\langle 0|, \quad \hat{\sigma}_2 = -i\,|0\rangle\langle 1| + i\,|1\rangle\langle 0|, \quad \hat{\sigma}_3 = |0\rangle\langle 0| - |1\rangle\langle 1|$$

form the Pauli basis in $L(\mathcal{H})$. Recall that

$$\begin{gathered} \operatorname{tr}\hat{\sigma}_k = 0, \quad \hat{\sigma}_k^2 = \hat{\sigma}_0, \\ \{\hat{\sigma}_k, \hat{\sigma}_l\} = 0, \quad [\hat{\sigma}_k, \hat{\sigma}_l] = 2i\operatorname{sign}(\pi)\hat{\sigma}_m, \quad (klm) = \pi(123), \end{gathered} \tag{1}$$

where $\pi(123)$ is a permutation of $\{1,2,3\}$, $k,l,m \in \{1,2,3\}$; $[\,,]$ and $\{\,,\}$ denote the commutator and anticommutator respectively.

The *Pauli basis* in $L(\mathcal{H}_n)$ is defined by

$$\left\{\hat{\sigma}_{k_1\ldots k_n}\right\}_{k_1,\ldots,k_n\in\{0,1,2,3\}}, \quad \hat{\sigma}_{k_1\ldots k_n} = \hat{\sigma}_{k_1}\otimes\ldots\otimes\hat{\sigma}_{k_n}, \tag{2}$$

where $\hat{\sigma}_{0\ldots0}$ is the identity operator. It is obvious that the Pauli basis consists of 4^n elements. We will use compact notations like $\hat{\sigma}_K = \hat{\sigma}_{k_1\ldots k_n}$, denoting the string $k_1\ldots k_n$, $k_1,\ldots,k_n \in \{0,1,2,3\}$, by the corresponding decimal representation K, $0 \leqslant K \leqslant 4^n-1$. Note that all the operators $\hat{\sigma}_K$ are Hermitian and unitary at the same time. In addition, one can easily check the useful relations

$$\hat{\sigma}_K^2 = \hat{\sigma}_{0\ldots0}, \quad \left\{\operatorname{tr}\hat{\sigma}_K\right\}_{K\neq0} = 0, \quad \operatorname{tr}\hat{\sigma}_{0\ldots0} = 2^n. \tag{3}$$

In what follows, we often use the symbol $\hat{I}$ to denote $\hat{\sigma}_{0\ldots0}$, if its meaning is clear from the context.

The following proposition is a direct consequence of relations (1): *any two operators of the Pauli basis, say $\hat{\sigma}_K$ and $\hat{\sigma}_L$, either commute or anticommute, that is*,

$$\textit{either}\ \ [\hat{\sigma}_K,\hat{\sigma}_L] = 0\ \ \textit{or}\ \ \ \{\hat{\sigma}_K,\hat{\sigma}_L\} = 0. \tag{4}$$

The strings $K = k_1\ldots k_n$ and $L = l_1\ldots l_n$ completely define the corresponding Pauli operators $\hat{\sigma}_K$ and $\hat{\sigma}_L$. Let p be the number of pairs (k_α, l_α), where $k_\alpha \in K$ and $l_\alpha \in L$, such that $k_\alpha \neq 0$, $l_\alpha \neq 0$, and $k_\alpha \neq l_\alpha$, $\alpha = 1,2,\ldots,n$. *If p is even (odd), then the operators commute (respectively, anticommute).* The proof of this statement is elementary.

The statement (4), which can be rewritten in the form $\hat{\sigma}_L\hat{\sigma}_K\hat{\sigma}_L = \pm\hat{\sigma}_K$, play a key role in implementation of our algorithm presented in the next section. Note also that Hamiltonians and density operators, being Hermitian, are written as linear combinations of the Pauli basis operators with *real* coefficients.

3. Decompositions of Hamiltonians in the Pauli basis

The simplest version of the Lie–Trotter–Suzuki decomposition has the form

$$e^{\tau H} = (e^{\tau H_1/m}e^{\tau H_2/m}\ldots e^{\tau H_r/m})^m + O(\tau^2 r^2/m).$$

In practice, one usually uses an enhanced formula of forth order, which gives an error of order $O(\tau^5 r^5/m^4)$, however, in any case, the operator exponentials in the product must be calculated with very high accuracy. Note that if these exponentials can be represented analytically in a simple closed form, it may be possible to reduce the exponential complexity to polynomial.

In Hamiltonian simulation, the first step as always is to divide, in some "maximal" way, the original Hamiltonian into pairwise commuting Hermitian parts, so that the total operator exponential will be found as the product of the exponentials of these partial Hamiltonians. Let $\hat{H}$ be such a partial

Hamiltonian. In what follows, we require that it can be represented as the sum

$$\hat{H} = \sum_{k=1}^{K} a_k \hat{H}_k, \quad a_k \in \mathbb{R}, \tag{5}$$

where the operators $\hat{H}_k$ are Hermitian and satisfy the conditions

$$\{\hat{H}_k, \hat{H}_l\}_{k \leqslant l} = b_m \hat{H}_m, \quad b_m \in \mathbb{R}, \quad k, l, m \in \{1, 2, \dots, K\}. \tag{6}$$

In addition, we assume that $K \ll 4^n$, since otherwise this decomposition does not have any meaningful sense. In formula (6), the integer-valued function $m = m(k, l)$ completely defines the anticommutation relations. Therefore, from a purely computational point of view, our algorithm reduces to an iterative procedure for this function and finite summation operations. Indeed, the next step obviously consists in computing the powers of $\hat{H}$. The second power is

$$\hat{H}^2 = \sum_{k \leqslant l} a_k a_l b_{m(k,l)} \hat{H}_{m(k,l)},$$

so that, after collecting similar terms, we obtain the decomposition of the form (5) with other coefficients, say c_k. Then the third power (and analogously the fourth one) of $\hat{H}$ has the form

$$\hat{H}^3 = \sum_{k \leqslant l} a_k c_l b_{m(k,l)} \hat{H}_{m(k,l)}.$$

It is important that the series of coefficients at the powers of the operator can often be summarized into a simple closed expression.

The proposed algorithm starts with the decomposition of the Hamiltonian in accordance with the expressions (5) and (6). Here the conditions (6) seem to be very strong. However, first, they are automatically satisfied for any set of anticommuting Pauli basis operators and, therefore, are of great significance in applications. Second, the model Hamiltonian of a quantum system often has a high degree of symmetry. It takes place, for example, under the quite weak assumption that there exists some sufficiently large permutation group, acting on qubits, such that the Hamiltonian is invariant with respect to this action. In the latter case, the conditions (6) usually hold and, moreover, the terms in the decomposition (5) have a number of common eigenvectors. And third, for Ising-type Hamiltonians, the corresponding lattice, as a rule, can be partitioned in some suitable way into local subsets for which the conditions (6) hold.

In conclusion of this section, we consider a special but very important version of the conditions (6) when

$$\hat{H}_k^2 = \hat{I}, \quad \{\hat{H}_k, \hat{H}_l\}_{k \neq l} = 0, \quad k, l = 1, 2, \dots, \tag{7}$$

where we formally add the identity operator $\hat{I} = \hat{H}_0$ to the set $\{\hat{H}_k\}_{k=1}^K$ to keep it closed under the anticommutation operation. In this case, an elementary calculation gives the following relations for the powers of $\hat{H}$:

$$\hat{H}^{2k+1} = a^{2k}\hat{H}, \quad \hat{H}^{2k} = a^{2k}\hat{I}, \quad k = 1, 2, \dots, \quad a = \left(\sum_{k=1}^{K} a_k^2\right)^{1/2}.$$

From the power series expansion, the exponential of the Hamiltonian (5), in its turn, can now be obtained in a simple closed form:

$$\exp\left(\tau\hat{H}\right) = \hat{I} + \tau\hat{H} + \frac{\tau^2}{2!}\hat{H}^2 + \frac{\tau^3}{3!}\hat{H}^3 + \frac{\tau^4}{4!}\hat{H}^4 + \dots =$$

$$= \left(\hat{I} + \frac{a^2\tau^2}{2!}\hat{I} + \frac{a^4\tau^4}{4!}\hat{I} + \dots\right) + \left(\frac{a\tau}{a}\hat{H} + \frac{a^3\tau^3}{a3!}\hat{H} + \dots\right) =$$

$$= \operatorname{ch}(a\tau)\hat{I} + \frac{\operatorname{sh}(a\tau)}{a}\hat{H}. \quad (8)$$

It is appropriate to clarify the significance of the obtained formula by the fact that the relations (7) are automatically fulfilled if the decomposition (5) contains only anticommuting Pauli operators. Note also that there is one more important special case when, in addition to the conditions (6), the operators $\hat{H}_k$ commute pairwise, $[\hat{H}_k, \hat{H}_l] = 0$ (the next section deals with just such a case). Then the exponential $\exp\left(\tau\hat{H}\right)$ is the product of exponentials $\exp\left(\tau a_k \hat{H}_k\right)$ of partial Hamiltonians, and each exponential can be calculated using a simple version of the basic algorithm and naturally represented as a linear combination of the operators $\hat{H}_k$. Then the product should be expanded into a linear combination of all the same operators.

4. Three-qubit model Hamiltonians

In the literature, there are many examples of few-qubits (usually two- and three-qubits) systems with various model Hamiltonians (see e.g. [8] and the references therein). In this section, we consider a three-qubit cluster and three model Hamiltonians describing different types of internal interaction between the qubits. The most important distinctive feature of these Hamiltonians is the presence of three-qubit interactions. In order to perform all calculations in an analytical form and thereby provide an illustrative example of using our algorithm, the Hamiltonians are chosen to be invariant under permutations of qubits. Namely, we define two Hamiltonians (the third one is $\hat{H}_1 + \hat{H}_2$) by the relations

$$\hat{H}_1 = \frac{1}{12}\left(\hat{F}_1 + \hat{F}_2 + \hat{F}_3 + 3\hat{S}\right), \quad \hat{H}_2 = \frac{1}{12}\left(\hat{G}_1 + \hat{G}_2 + \hat{G}_3 + 3\hat{I}\right). \quad (9)$$

where $\hat{S} = -\hat{\sigma}_{333}$, and

$$\hat{F}_1 = \hat{\sigma}_{113} + \hat{\sigma}_{131} + \hat{\sigma}_{311}, \quad \hat{F}_2 = \hat{\sigma}_{223} + \hat{\sigma}_{232} + \hat{\sigma}_{322}, \quad \hat{F}_3 = \hat{\sigma}_{003} + \hat{\sigma}_{030} + \hat{\sigma}_{300},$$

$\hat{G}_1 = \hat{\sigma}_{022}+\hat{\sigma}_{202}+\hat{\sigma}_{220}, \quad \hat{G}_2 = \hat{\sigma}_{011}+\hat{\sigma}_{101}+\hat{\sigma}_{110}, \quad \hat{G}_3 = -\hat{\sigma}_{033}-\hat{\sigma}_{303}-\hat{\sigma}_{330}.$

Given the symmetry, one can easily obtain the relations

$$\{\hat{F}_i, \hat{S}\} = 2\hat{G}_i, \quad \{\hat{G}_i, \hat{S}\} = 2\hat{F}_i, \quad i = 1, 2, 3,$$

$$\{\hat{F}_i, \hat{F}_j\} = 2\hat{G}_k, \quad \{\hat{G}_i, \hat{G}_j\} = 2\hat{G}_k, \quad \{\hat{F}_i, \hat{G}_j\} = 2\hat{F}_k, \quad i \neq j \neq k,$$

$$\{\hat{F}_1, \hat{G}_1\} = 6\hat{S} + 4\hat{F}_1, \quad \{\hat{F}_2, \hat{G}_2\} = 6\hat{S} + 4\hat{F}_2, \quad \{\hat{F}_3, \hat{G}_3\} = 6\hat{S} - 4\hat{F}_3.$$

The squares of the operators are $\hat{S}^2 = \hat{I}$ and

$$\hat{F}_1^2 = \hat{G}_1^2 = 3\hat{I} + 2\hat{G}_1, \quad \hat{F}_2^2 = \hat{G}_2^2 = 3\hat{I} + 2\hat{G}_2, \quad \hat{F}_3^2 = \hat{G}_3^2 = 3\hat{I} - 2\hat{G}_3.$$

Using these relations, we find that the Hamiltonians $\hat{H}_1$ and $\hat{H}_2$ commute, $[\hat{H}_1, \hat{H}_2] = 0$, and

$$\{\hat{H}_1, \hat{H}_2\} = 2\hat{H}_1, \quad \hat{H}_1^2 = \hat{H}_2^2 = \hat{H}_2, \tag{10}$$

so that

$$\hat{H}_1^3 = \hat{H}_1, \;\; \hat{H}_1^4 = \hat{H}_2, \;\; \hat{H}_1^5 = \hat{H}_1, \ldots, \quad \hat{H}_2^3 = \hat{H}_2, \quad \hat{H}_2^4 = \hat{H}_2, \ldots.$$

Finally, using the above relations and the Taylor series expansion of the operator exponential, we obtain

$$\exp\left(\tau\hat{H}_1\right) = \hat{I} + \tau\hat{H}_1 + \frac{\tau^2}{2}\hat{H}_1^2 + \frac{\tau^3}{3!}\hat{H}_1^3 + \frac{\tau^4}{4!}\hat{H}_1^4 + \frac{\tau^5}{5!}\hat{H}_1^5 + \cdots =$$

$$= \hat{I} + \left(\tau + \frac{\tau^3}{3!} + \frac{\tau^5}{5!} + \cdots\right)\hat{H}_1 - \hat{H}_2 + \left(1 + \frac{\tau^2}{2} + \frac{\tau^4}{4!} + \cdots\right)\hat{H}_2 =$$

$$= \hat{I} + \mathrm{sh}\tau\hat{H}_1 + (\mathrm{ch}\tau - 1)\hat{H}_2, \tag{11}$$

and analogously,

$$\exp\left(\tau\hat{H}_2\right) = \hat{I} + (\mathrm{e}^\tau - 1)\hat{H}_2. \tag{12}$$

We will also consider the Hamiltonian

$$\hat{H} = \hat{H}_1 + \hat{H}_2, \tag{13}$$

for which the corresponding exponential is

$$\exp\left(\tau\hat{H}\right) = \hat{I} + \mathrm{e}^\tau\mathrm{sh}\tau\hat{H}_1 + \mathrm{e}^\tau\,(\mathrm{ch}\tau - 1)\hat{H}_2. \tag{14}$$

The Hamiltonians (9) and (13) have the same eigenvectors, but of course their eigenvalues must be different. We also have the following consequence of the symmetry of $\hat{H}_1$, $\hat{H}_2$, and $\hat{H}$: if a state is invariant under all permutations

of qubits, then it is obviously the eigenvector of these Hamiltonians. This implies that the states

$$S_0 = |000\rangle\,, \quad S_1 = |111\rangle\,,$$
$$W = \frac{|001\rangle + |010\rangle + |100\rangle}{\sqrt{3}}, \quad \widetilde{W} = \frac{|011\rangle + |101\rangle + |110\rangle}{\sqrt{3}},$$

are eigenvectors for them, where W is one of the two inequivalent classes of completely entangled states, and $\widetilde{W}$ is the "false", W-state. Other four eigenvectors can be chosen as

$$V_1 = \frac{2\,|001\rangle - |010\rangle - |100\rangle}{\sqrt{6}}, \quad V_2 = \frac{|010\rangle - |100\rangle}{\sqrt{2}},$$
$$V_3 = \frac{2\,|011\rangle - |101\rangle - |110\rangle}{\sqrt{6}}, \quad V_4 = \frac{|101\rangle - |110\rangle}{\sqrt{2}}.$$

These eight eigenvectors make up an orthonormal basis in the Hilbert space $\mathcal{H}^{\otimes 3}$. The Hamiltonians (9) and (13) have strongly degenerate spectra. By introducing the notations $[S] = \{S_0, S_1\}$ and $[V] = \{V_1, V_2, V_3, V_4\}$, we can write down these spectra as

$$\mathrm{Spec}\,\hat{H}_1 = \{\,(-1, \widetilde{W}),\, (0, [S], [V]),\, (1, W)\}, \tag{15}$$

$$\mathrm{Spec}\,\hat{H}_2 = \{(0, [S], [V]),\, (1, W, \widetilde{W})\}, \tag{16}$$

$$\mathrm{Spec}\,\hat{H} = \{(0, [S], [V], \widetilde{W}),\, (2, W)\}, \tag{17}$$

where the real numbers in round parentheses denote the corresponding eigenvalues.

5. Three-qubit cluster in a thermal environment

Model Hamiltonians provide wide possibilities for approximate simulation of real quantum systems in condensed matter physics. This section is devoted to a toy model of a material consisting of three-qubit clusters with strong intracluster quantum coherence and a weak (thermal) intercluster interaction. Such models of clusters in the presence of a thermal environment were considered earlier for two-qubit clusters [9] and three and four-qubit clusters [10–12] with simpler but less symmetric Hamiltonians. We will use the Hamiltonians that were studied in the previous section.

In general, the total Hamiltonian of a subsystem and a thermal environment (bath), weakly coupled with each other, is given by the sum

$$\hat{H} = \hat{H}_s + \hat{H}_b + \hat{H}_{int}.$$

In this connection, there arises a subtle issue whether the density operator of the subsystem, $\rho(t)$, given in an arbitrary initial state $\rho(0)$, will come to an equilibrium (Gibbs) state over long time. For Hamiltonians with nondegenerated spectrum, von Neumann proves this statement rigorously in his

pioneer paper [13] (see also [14, 15]). However, it is shown in [16] that the requirement of non-degeneracy can be ruled out; in this case, the subsystem will reside close to a fixed equilibrium state most of the time. Also, there are no theoretical or experimental examples of degenerate subsystems with non-equilibrium long time dynamics in the literature. On the other hand, the degeneracy is a consequence of the high symmetry of the subsystem's Hamiltonian, but in realistic situations, perturbations violate the degeneracy of energy level [17]. Our consideration will be based on the following assumption: if the intensity of the interaction (in the sense of the usual operator norm of $\hat{H}_{int}$) between the subsystem and the environment is much less than the temperature $1/\beta$, and the internal interaction (determined by H_s) of qubits in the subsystem is greater than $1/\beta$, then the subsystem will be in a state being very close to the Gibbs state $\hat{\rho} = \exp\bigl(-\beta\hat{H}_s\bigr)/Z$.

At this stage, we have to introduce a dimensional factor into the Hamiltonians (9) and (13) by replacing $\hat{H} \to \omega\hat{H}$ or, equivalently, by setting $\tau = -\beta\omega$, where $[\omega] = L^{-1}$; in other words, the coefficient $1/12$ in (9) will be replaced by $\omega/12$. According to formulae (15)–(17), the eigenvalues of the Hamiltonians $\hat{H}_1$, $\hat{H}_2$, and $\hat{H}$ are $\{-\omega, 0, \omega\}$, $\{0, \omega\}$, and $\{0, 2\omega\}$, respectively. For the interaction $\hat{H}_1$, the ground state of the system is non-degenerated, as well as the exited state for $\hat{H}$, while both the states for the Hamiltonian $\hat{H}_2$ are degenerated. From the expressions (11), (12), and (14), one can find the corresponding partition functions $Z = \operatorname{tr}\exp\bigl(-\beta\hat{H}\bigr)$ and density operators $\hat{\rho} = \exp\bigl(-\beta\hat{H}\bigr)/Z$. Taking into account that $\operatorname{tr}\hat{H}_1 = 0$ and $\operatorname{tr}\hat{H}_2 = 2\omega$, we obtain

$$
\begin{gathered}
Z_1 = 6 + 2\operatorname{ch}(\omega\beta), \quad Z_2 = 6 + 2\mathrm{e}^{-\omega\beta}, \quad Z = 9 - 2\mathrm{e}^{-\omega\beta} + \mathrm{e}^{-2\omega\beta}, \\
\hat{\rho}_1 = \frac{1}{Z_1}\left[\hat{I} - \frac{\operatorname{sh}(\omega\beta)}{\omega}\hat{H}_1 + \frac{\operatorname{ch}(\omega\beta) - 1}{\omega}\hat{H}_2\right], \\
\hat{\rho}_2 = \frac{1}{Z_2}\left[\hat{I} + \frac{\mathrm{e}^{-\omega\beta} - 1}{\omega}\,\hat{H}_2\right],
\end{gathered}
\tag{18}
$$

$$
\hat{\rho} = \frac{1}{Z}\left[\hat{I} - \frac{\mathrm{e}^{-\omega\beta}\operatorname{sh}(\omega\beta)}{\omega}\hat{H}_1 + \frac{\mathrm{e}^{-\omega\beta}(\operatorname{ch}(\omega\beta) - 1)}{\omega}\,\hat{H}_2\right]. \tag{19}
$$

We see that the partition function Z_1 diverges in the low temperature limit. In a real system, the divergence will be compensated by the sharp dominance of the Hamiltonian H_{int} in comparison with the temperature. In fact, the condition of weak coupling between the cluster and its thermal environment is violated for all the three types of interaction in the region $\beta \gg 1$. Therefore, there are no equilibrium states despite of good definiteness of the density operators: for $\beta \to \infty$, we have (with the same error $O(\mathrm{e}^{-\omega\beta})$)

$$
\hat{\rho}_1 = \frac{\hat{H}_2 - \hat{H}_1}{2\omega}, \quad \hat{\rho}_2 = \frac{\hat{I}}{6} - \frac{\hat{H}_2}{6\omega}, \quad \hat{\rho} = \frac{\hat{I}}{9} + \frac{\hat{H}_2 - \hat{H}_1}{18\omega}.
$$

The divergence of Z_1 is reflected in the fact that $\hat{\rho}_1$ is a pure state in the zero temperature limit, $\hat{\rho}_1^2 = \hat{\rho}_1$, so that it cannot represent any Gibbs state. An analogous picture takes place at high temperatures. In this case, the internal interaction between qubits becomes of the order of $1/\beta$ or less than it, so that the cluster again cannot be considered in isolation from the entire system. In the region $\beta \ll 1$ where quantum effects no longer dominate, we have the usual semiclassical behavior (in particular, all eigenstates are almost equally probable)

$$\hat{\rho} = \hat{\rho}_1 = \frac{\hat{I} - \beta\hat{H}_1}{8} + O(\beta^2), \quad \hat{\rho}_2 = \frac{4 + \omega\beta}{32}\hat{I} - \frac{\beta}{8}\hat{H}_2 + O(\beta^2), \quad \beta \to 0.$$

Using the well-known expressions for the average energy, von Neumann entropy, and free energy,

$$\mathcal{E} = \operatorname{tr}(\hat{\rho}\hat{H}) = -\partial_\beta \ln Z, \quad S = \ln Z + \beta\mathcal{E}, \quad \mathcal{F} = \mathcal{E} - TS = -\frac{1}{\beta}\ln Z, \quad (20)$$

we have plotted in figures 1 and 2, respectively, the entropies and free energies for the three states under considerations. Recall that the transition from natural units to ordinary units consists in the replacements

$$\beta \to \frac{\beta}{c\hbar}, \quad \omega \to c\hbar\omega.$$

Thus the value $\beta = 1$ corresponds to the inverse temperature $1/T \approx 3 \cdot 10^{16}\,\mathrm{erg}^{-1}$, that is, $T \approx 3 \cdot 10^{-17}\,\mathrm{erg} \approx 0.2\,\mathrm{K}$. Note that the usual working inverse temperatures of qubits, realized, for example, in the form of quantum dots or superconducting artificial atoms, are in the interval $0.2 \leqslant \beta \leqslant 2$.

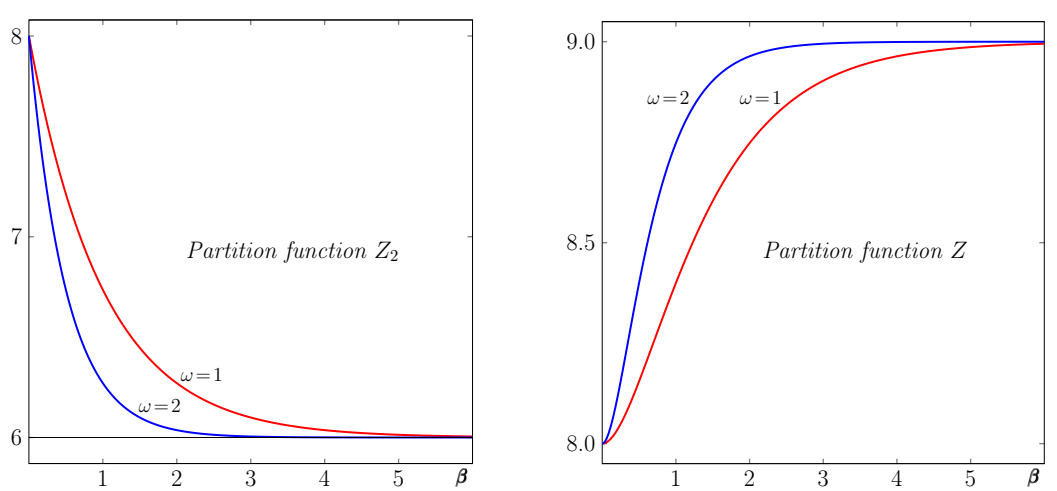

Figure 1. In the low temperature region, $\lim\limits_{\omega\to\infty} Z_2 = 6$ and $\lim\limits_{\omega\to\infty} Z = 9$, in contrast to the partition function Z_1, which diverges

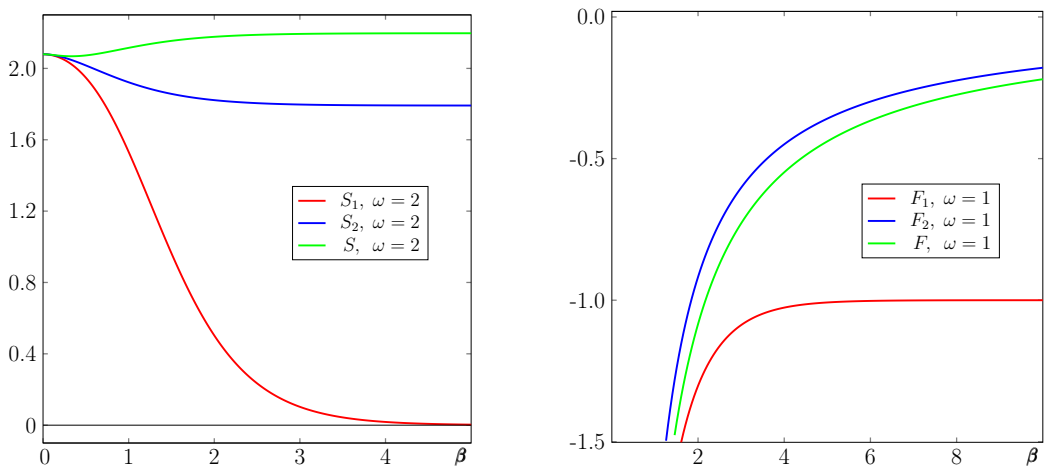

Figure 2. Entropy $S(\beta)$ (left panel) and free energy $F(\beta)$ (right panel) for the states (18) and (19). In the low temperature limit $\beta \to \infty$, we have, with an error $O(\mathrm{e}^{-2\omega\beta})$, the expansions $F_1 = -\omega - (6/\beta)\mathrm{e}^{-\omega\beta}$, $F_2 = -(\ln 6)/\beta - \mathrm{e}^{-\omega\beta}/(3\beta)$, $F = -(\ln 9)/\beta + 2\mathrm{e}^{-\omega\beta}/(9\beta)$. In the high temperature limit $\beta \to 0$, we have $F_1 \sim F_2 \sim F \sim -3(\ln 2)/\beta$

6. Conclusions

We have presented a simple method for simulating multi-qubit clusters having Hamiltonians of a special form, but nevertheless covering a wide range of quantum systems in condensed matter physics. It is assumed that the Hamiltonian of a quantum system can be represented as a linear combination of some set of partial Hamiltonians, so that their anticommutators up to a factor are themselves elements of this set. Another feature of our approach is the use of the Pauli basis, in which all calculations have the simplest form. To demonstrate the effectiveness of the main algorithm, we considered a cluster of three qubits and three model Hamiltonians representing various types of interactions that are symmetric under permutations of qubits and therefore make possible a fully analytical treatment.

Our algorithm was used to find the density operator, partition function, entropy, and free energy of such a cluster, weakly coupled to a thermal environment, for the Hamiltonians under consideration. In our model, the cluster is in a Gibbs state in the temperature interval 0.1−2 K, that is, in the operating range of modern quantum processors. Our analysis showed that the thermodynamic properties of such a system strongly depend on the type of internal interaction of qubits in the cluster.

References

[1] J. Preskill, "Quantum Computing in the NISQ era and beyond," *Quantum*, vol. 2, p. 79, 2018. DOI: 10.22331/q-2018-08-06-79.

[2] S. McArdle, S. Endo, A. Aspuru-Guzik, S. C. Benjamin, and X. Yuan, "Quantum computational chemistry," *Reviews of Modern Physics*, vol. 92, no. 1, 2020. DOI: 10.1103/revmodphys.92.015003.

[3] G. H. Low and I. L. Chuang, "Hamiltonian simulation by qubitization," *Quantum*, vol. 3, p. 163, 2019. DOI: 10.22331/q-2019-07-12-163.

[4] B. Zeng, X. Chen, D.-L. Zhou, and X.-G. Wen, *Quantum Information Meets Quantum Matter*. Springer New York, 2019. DOI: 10.1007/978-1-4939-9084-9.

[5] L. Bassman, M. Urbanek, M. Metcalf, J. Carter, A. F. Kemper, and W. A. de Jong, "Simulating quantum materials with digital quantum computers," *Quantum Science and Technology*, vol. 6, no. 4, p. 043 002, 2021. DOI: 10.1088/2058-9565/ac1ca6.

[6] D. W. Berry, A. M. Childs, R. Cleve, R. Kothari, and R. D. Somma, "Simulating Hamiltonian dynamics with a truncated Taylor series," *Physical Review Letters*, vol. 114, p. 090 502, 9 2015. DOI: 10.1103/PhysRevLett.114.090502.

[7] D. W. Berry, A. M. Childs, R. Cleve, R. Kothari, and R. D. Somma, "Exponential improvement in precision for simulating sparse Hamiltonians," in *Proceedings of the Forty-Sixth Annual ACM Symposium on Theory of Computing*, New York, NY, USA, 2014, pp. 283–292. DOI: 10.1145/2591796.2591854.

[8] I. M. Georgescu, S. Ashhab, and F. Nori, "Quantum simulation," *Reviews of Modern Physics*, vol. 86, pp. 153–185, 1 2014. DOI: 10.1103/RevModPhys.86.153.

[9] G. L. Deçordi and A. Vidiella-Barranco, "Two coupled qubits interacting with a thermal bath: A comparative study of different models," *Optics Communications*, vol. 387, pp. 366–376, 2017. DOI: 10.1016/j.optcom.2016.10.017.

[10] C. Boudreault, H. Eleuch, M. Hilke, and R. MacKenzie, "Universal quantum computation with symmetric qubit clusters coupled to an environment," *Physical Review A*, vol. 106, no. 6, p. 062 610, 2022. DOI: 10.1103/PhysRevA.106.062610.

[11] T. Menke *et al.*, "Demonstration of tunable three-body interactions between superconducting qubits," *Physical Review Letters*, vol. 129, no. 22, p. 220 501, 2022. DOI: 10.1103/PhysRevLett.129.220501.

[12] V. Verma and M. Sisodia, "Two-way quantum communication using four-qubit cluster state: Mutual exchange of quantum information," *Modern Physics Letters A*, vol. 37, no. 04, p. 2 250 020, 2022. DOI: 10.1142/S0217732322500201.

[13] J. Von Neumann, "Proof of the ergodic theorem and the H-theorem in quantum mechanics: translation in English," *European Physical Journal H*, vol. 35, pp. 201–235, 2010.

[14] A. Kossakowski, A. Frigerio, V. Gorini, and M. Verri, "Quantum detailed balance and KMS condition," *Communications in Mathematical Physics*, vol. 57, no. 2, pp. 97–110, 1977.

[15] G. Bulnes Cuetara, M. Esposito, and G. Schaller, "Quantum thermodynamics with degenerate eigenstate coherences," *Entropy*, vol. 18, no. 12, 2016. DOI: 10.3390/e18120447.

[16] A. Short and T. Farrelly, "Quantum equilibration in finite time," *New Journal of Physics*, vol. 14, no. 1, p. 013 063, 2012. DOI: 10.1088/1367-2630/14/1/013063.

[17] M. A. Novotny, F. Jin, S. Yuan, S. Miyashita, H. De Raedt, and K. Michielsen, "Quantum decoherence and thermalization at finite temperature within the canonical-thermal-state ensemble," *Phys. Rev. A*, vol. 93, no. 3, p. 032 110, 2016. DOI: 10.1103/PhysRevA.93.032110.

For citation:

E. L. André, A. N. Tsirulev, Hamiltonian simulation in the Pauli basis of multi-qubit clusters for condensed matter physics, Discrete and Continuous Models and Applied Computational Science 31 (3) (2023) 247–259. DOI: 10.22363/2658-4670-2023-31-3-247-259.

Information about the authors:

André, Eduardo L. — PhD student, Department of Applied Physics, Tver State University, Russia (e-mail: lumonansoni@gmail.com, phone: +7(4822)322839, ORCID: https://orcid.org/0000-0002-0697-1639)

Tsirulev, Alexander N. — Doctor of Sciences in Physics and Mathematics, Professor of the Department of General Mathematics and Mathematical Physics, Tver State University, Russia (e-mail: tsirulev.an@tversu.ru, phone: +7(4822)585683, ORCID: https://orcid.org/0000-0003-4168-3613, Scopus Author ID: 16409936300)

УДК 514.74:530.145
PACS 03.65.Fd, 03.65.Ca, 02.10.Ud,
DOI: 10.22363/2658-4670-2023-31-3-247-259
EDN: KRDBEG

Моделирование в базисе Паули гамильтонианов многокубитных кластеров физики конденсированного состояния

Э. Л. Андре[1,2], **А. Н. Цирулев**[1]

[1] *Факультет естественных наук, университет им. Агостиньо Нето, Проспект 4 февраля, д. 7, Луанда, Ангола*
[2] *Математический факультет, Тверской государственный университет, Садовый пер., д. 35, Тверь, 170002, Россия*

Аннотация. Предлагается эффективный метод математического моделирования гамильтонианов многокубитных квантовых систем с взаимодействием специального вида. В нашем подходе гамильтониан системы n кубитов должен быть представлен линейной комбинацией в стандартном базисе Паули, а затем разложен в сумму частичных гамильтонианов, которые, вообще говоря, не являются операторами Паули и удовлетворяют некоторым антикоммутационным соотношениям. Для трёх типов гамильтонианов, инвариантных относительно перестановок кубитов, эффективность основного алгоритма в модели трёхкубитного кластера показана посредством вычисления операторных экспонент этих гамильтонианов в явном аналитическом виде. Кроме того, вычислен оператор плотности состояния, статистическая сумма, энтропия и свободная энергия для кластера, слабо связанного с термостатом. В нашей модели кластер находится в состоянии Гиббса в интервале температур 0,1—2 K, что соответствует рабочему диапазону современных квантовых процессоров. Из нашего анализа следует, что термодинамические свойства такой системы сильно зависят от типа внутреннего взаимодействия кубитов в кластере.

Ключевые слова: моделирование квантовых гамильтонианов, кластер кубитов, операторная экспонента, термостат, состояние Гиббса, термодинамические свойства

Discrete & Continuous Models
& Applied Computational Science
ISSN 2658-7149 (online), 2658-4670 (print)

2023, 31 (3) 260–272
http://journals.rudn.ru/miph

Research article

UDC 519.872:519.217
PACS 07.05.Tp, 02.60.Pn, 02.70.Bf
DOI: 10.22363/2658-4670-2023-31-3-260-272
EDN: KIJKGU

Identification of COVID-19 spread factors in Europe based on causal analysis of medical interventions and socio-economic data

Kouame A. Brou

Peoples' Friendship University of Russia (RUDN University)
6, Miklukho-Maklaya str., Moscow, 117198, Russian Federation

(received: May 30, 2023; revised: July 25, 2023; accepted: September 8, 2023)

Abstract. Since the appearance of COVID-19, a huge amount of data has been obtained to help understand how the virus evolved and spread. The analysis of such data can provide new insights which are needed to control the progress of the epidemic and provide decision-makers with the tools to take effective measures to contain the epidemic and minimize the social consequences. Analysing the impact of medical treatments and socioeconomic factors on coronavirus transmission has been given considerable attention. In this work, we apply panel autoregressive distributed lag modelling (ARDL) to European Union data to identify COVID-19 transmission factors in Europe. Our analysis showed that non-medicinal measures were successful in reducing mortality, while strict isolation virus testing policies and protection mechanisms for the elderly have had a positive effect in containing the epidemic. Results of Dumitrescu–Hurlin paired-cause tests show that a bi-directional causal relationship exists for all EU countries causal relationship between new deaths and pharmacological interventions factors and that, on the other hand, some socioeconomic factors cause new deaths when the reverse is not true.

Key words and phrases: causality analysis, COVID-19, socio-economic, Dumitrescu–Hurlin' panel

1. Introduction

In January 2020, the SARS-CoV-2 coronavirus from 2019 made its way to Europe. As a result, the European Union and the majority of European nations had documented their first case. It should be observed, nevertheless, that the infection spread unevenly. At the end of April, there were more than three million confirmed cases of the severe acute respiratory syndrome coronavirus (COVID-19) worldwide (CSS, 2020), (SARS-CoV-2). The first human instance of the coronavirus was discovered in Wuhan, China, in late 2019 despite the fact that its origins are still unknown. One way the

coronavirus is spread from person to person is through respiratory droplets created when infected people cough or sneeze in front of others [1].

Air travel is one of the factors contributing to the coronavirus outbreak in Europe. Late January or early February saw the confirmation of the first instances. Human contacts after the virus's introduction to Europe helped it spread quickly. Social contact is crucial for the spread of all viruses, including COVID-19, according to research [2]. Human behavior is frequently viewed as a crucial safeguard for stopping the COVID-19 pandemic [3]. Globally, policymakers and health professionals are urging people to exercise social responsibility by limiting social interaction, adhering to stringent cleanliness and distancing guidelines, and being vaccinated. 1 Politicians are advising their constituents to weigh the social costs of their individual acts in terms of economics. In order to counteract COVID-19, official strategies heavily rely on this method of using social capital. The significance of social capital to controlling COVID-19 and preserving population health, however, is not well supported by systematic studies. According to what we know, this study is the first to rigorously analyze the dynamic link between social capital and health outcomes, as determined by COVID-19 instances and excess mortality. We systematically demonstrate that social capital has a causal and beneficial impact on pandemic-related health outcomes based on different analyses for seven European nations: Austria, Germany, Great Britain, Italy, the Netherlands, Sweden, and Switzerland. Personal hygiene habits and non-pharmaceutical interventions are the only ways to stop the spread of COVID-19 in the absence of vaccines and medications.

The development of a broad framework for the causal analysis of COVID-19 in Europe is the goal of this research. As response variables, the number of new cases and fatalities attributable to COVID-19 are used. Potential causative variables include intervention factors and measures.

2. Related works

Several studies have used various approaches and linked data from the WHO and other COVID-19 data sources to study the pandemic's spread or serve as a guide for developing measures. Using the COVID-19 government response tracker data from the University of Oxford, employed Nonlinear Additive Noise Models for Bivariate Causal Discovery to determine the causative effect of a factor or an intervention measure on the number of new cases or an intervention measure. Reference [4] used data from the pandemic that affected 31 provinces and regions in China from January 20, 2020, to February 24, 2021, and the directed acyclic graph to demonstrate the causal link between influencing factor and daily cases. Using information from the official reports of the Robert Koch Institute, [5] studied the spread of the virus in Germany and the causative influence of restriction measures. In order to estimate the total causal effects based on directed acyclic graph analysis by negative binomial regression, collected data for 401 German districts between 15 February and 8 July 2020 from publicly accessible sources in Germany (e.g., the Robert Koch Institute, Germany's National Meteorological Service, Google). The most commonly used statistical methods for analysing epidemiological factors of COVID-19 and evaluating intervention measures include correlation, regression, logistic regression and a dynamic model coupled with a linear model. Yet, if particular structures are considered, statistical methods like

regression can only be regarded as instruments for causal analysis because they only allow a measure of causal dependence to be defined for these structures. On the basis of natural hypotheses, a procedure that is more effective than those now in use can be developed. Based on association analysis, this technique is known as dependency analysis. The statistical examination of the impacts of influencing factors and health interventions on the dissemination of COVID-19 has used association analysis as a reference. Yet, it is still challenging to comprehend the COVID-19 transmission pathway based on association analysis. The data were taken from the GlobalEconomy.com website used Pearson correlation analysis and multivariate linear regression to uncover economic and socio-political aspects that could fuel the coronavirus's expansion.

3. Materials and methods

3.1. Data Description

The analysis includes data for European economies from February 1st, 2020, through November 27th, 2022. Based on the statistics that are available, the era and the group of nations are chosen. The University of Oxford's COVID-19 government response was where the information came from. The Government Response Index can be created using the data in this set, which also includes a stringency index, a containment and health index, and an economic support index (see table 1).

Table 1

Definition of variables

Variables	Definition
NEW_DEATHS	News recorded deaths of COVID 19
STRINGENCY	Stringency Index
CONTAINMENT	Containment Health Index
ECONOMIC_SUP	Economic Support Index
VACCINATION	Vaccination policy
TESTING	Availability of detection
PROTECT_ELD	Care policy for the elderly population

The stringency index collects data on social segregation measures, coded from eight indicators: stay-at-home regulations, workplace closures, public event cancellations, gathering size restrictions, closures to public transportation, and travel restrictions both domestically and internationally.

Three indices that stand for public awareness efforts, testing regulations, and contact tracing make up the containment and health index. The index stands for the government's emergency health system policies, including the coronavirus testing program.

The government's income support program for citizens in times of crisis is reflected in the economic support index, which consists of two indicators:

household anticipated debt alleviation and government income assistance. Each of these three metrics is expressed as a simple sum of the values for the underlying metrics, scaled to a range between 0 and 100. These indexes are provided for comparison and shouldn't be used as a judgment on the suitability or efficacy of a nation's approach. The WHO is the source of the daily total of new cases. The time frame for the study is from January 1, 2020, to December 4, 2022, and it includes 230 different nations.

Table 2 displays a statistical breakdown of the key variables. The greatest value is 1623, the minimum value is 1918, and the average value is 42.27578, using the daily number of new deaths as an example. The number of new deaths is chosen as the explanatory variable since all efforts implemented by different governments around the world aim to prevent mortality, and reducing the number of cases will likely result in a decrease in deaths. So, the analysis will show us which measures not new instances as was noted in earlier literature really had an impact on pandemic related deaths.

Table 2

Descriptive and Summary Statistics

Variables	Mean	Standard Deviation	Minimum	Maximum
NEW_DEATHS	42.27578	104.4784	-1918.000	1623.000
STRINGENCY	43.11964	23.07557	0	96.30000
CONTAINMENT	49.82720	17.54525	0	90.00000
ECONOMIC_SUP	57.41835	34.87956	0	100.0000
VACCINATION	2.998873	2.247651	0	5.000000
TESTING	2.355943	0.799513	0	3.000000
PROTECT_ELD	1.588960	1.006744	0	3.000000

3.2. Methodology

In our empirical research, we examined how health interventions and socioeconomic observational data contributed to the global spread of COVID-19. Using this method, we may assess how health measures have affected the spread of COVID-19. In order to accomplish our goal, we used in this study a linear function that incorporates socioeconomic observational data and health treatments as an extra variable to control factors that are equivalent to COVID-19. As suggested by Pesaran and Shin, the equation is calculated using a time series autoregressive distributed lag model (ARDL). The advantage of the ARDL framework is that it can differentiate between short- and long-term impacts, which enhances earlier material. We may also predict a consistent short-term cross-sectional influence (short term coefficient of nations) due to our extensive sample size. Due to its distinction between short- and long-term impacts, the ARDL methodology aids in addressing the shortcomings of earlier work.

Using both time and cross-sectional dimensions increases the overall number of data and their variability in our panel estimation. A panel estimation also

reduces the noise that results from a single time-series estimation, leading to more trustworthy inference.

3.2.1. Panel unit root tests

The determination of the order of integration of variables serves as the foundation for estimating any econometric model. It is required to verify that the variables in the regression are either integrated of order zero $I(0)$ or at most integrated at order one I during the ARDL model estimate procedure $I(1)$. Reference [6] was used to check the integration of the variables in the proper sequence. The ADF regression for panel data serves as the foundation for these two tests and is described as follows in (1):

$$\Delta y_{i,t} = \omega_i y_{i,t-j} + \sum_{j=1}^{p} \phi_j \Delta y_{i,t-j} + \epsilon_{i,t}, \text{ where } \omega_i = \rho_i - 1. \tag{1}$$

Both tests evaluate the zero-unit root H_0: $\omega_i = 0$ ($\rho = 1$) with respect to the stationarity alternative H_1: $\omega_i < 0$ ($\rho_i < 1$). The LLC test assumes that the tested parameters are the same in all panels, i.e., $\rho_i = \rho$ for all countries in the panel. The IPS test, which averages the ADF statistic and enables the parameters to vary across panels, is less constrictive than the LLC test. However, because they do not take into consideration the cross-section dependency issue that could arise as a result of macroeconomic linkages, unexplained residual independence, and unobserved common factors, both the IPS and LLC tests are regarded as first-generation unit root tests. In order to determine whether the variables in the model for this study have any cross-sectional dependence, second-generation unit root tests are run. Then, the Pesaran [7] proposed cross-section dependence (CD) test is conducted. When N is more than T, the CD test can be used to determine whether there is any cross-sectional dependency among the variables. The pair correction coefficients of OLS residual regressions are averaged to form the basis of the CD test. After the CD test has confirmed whether cross-sectional dependence exists, the cross-sectional Augmented Dickey-Fuller (CADF) test is carried out by Pesaran [8]. In order to test the null hypothesis of cross-sectional dependency among a panel of nations, the CADF test considers cross-section dependence among the variables. This is done to verify that the variables are still either $I(0)$ or I even if there is cross-sectional dependency among the group of countries $I(1)$.

3.2.2. Panel cointegration tests

After the order of integration is established, the next step in the study is to test for evidence of long-run cointegration between NEW DEATHS and the independent variables using the panel cointegration tests from Pedroni, Kao and Westlund may be used for samples smaller than 100 in number. Based on the panel-data model for an $I(1)$ dependent variable y, the Pedroni and Kao tests compare the cointegration alternative to the null hypothesis of no cointegration (see (2)):

$$y_{i,t} = x'_{it}\beta_i + z'_{it}\tau_i + \epsilon_{i,t}, \tag{2}$$

where both tests demand that the covariates not be integrated among themselves for each panel I the variables in $x(i,t)$ are an $I(1)$ series. The Kao test constrains $\beta_i = \beta$ by assuming that all of the nations in the panel share a common cointegration vector. There are some distinctions between the two tests even though they both use the identical null and alternative hypotheses. In reality, the Pedroni test differs from the Kao test in that it accepts panel-specific cointegrating vectors.

3.2.3. Autoregressive distributed Lag model

The ARDL model is estimated via unit root and cointegration tests. The ARDL model can be employed with confidence for short sample periods and distinguishes between short- and long-run coefficients. In fact, [8] shows that the long-run parameters are super-consistent even with a small sample size, whereas the short-run values are $\sqrt{T}$ consistent. A panel ARDL (p, q_1, q_2, q_3, q_4, q_5) Equation is used to express the connection as a result, where p stands for the lags of the dependent variable and q for the lags of the independent variables. In (3), we can see a representation of the panel ARDL equation:

$$\Delta\text{NEW\_DEATHS}_{i,t} = \\ = \alpha_0 + \sum_{j=1}^{p} \alpha_{i,j}^{1} \Delta\text{NEW\_DEATHS}_{t-i} + \sum_{k=1}^{6} \sum_{j=0}^{qk} \alpha_{i,j}^{k+1} X_{t-j}^{k} + \epsilon_{i,t}, \quad (3)$$

where $i = 1, 2, 3, \ldots, N$ and $t = 1, 2, 3, \ldots, T$, α_i represents the fixed effects, X^k $\alpha_{i,j}^{k}$, $k = 1, 2, \ldots, 9$ are the lagged coefficients of the independent variables (Stringency Index, Containment Health Index, Economic Support, Vaccination policy, Testing policy, Protection to elderly) and the regressors and $\epsilon_{i,t}$ is the error term which is assumed to be white noise and varies across countries and time. In a panel error correction (ECM) representation equation (4) is formulated as follows:

$$\Delta\text{NEW\_DEATHS}_{i,t} = \alpha_i + \sum_{j=1}^{p} \alpha_{i,j}^{1} \Delta\text{NEW\_DEATHS}_{t-i} + \\ + \sum_{k=1}^{6} \sum_{j=0}^{qk} \alpha_{i,j}^{k+1} X_{t-j}^{k} + \sum_{k=1}^{6} \beta_k X_{t-i}^{k} + \epsilon_{i,t}, \quad (4)$$

where Δ is the first difference of variables. Also, α_1–α_7 are the short-run coefficients. While β_1–β_7 are the long-run coefficients of stringency index, containment health index, economic support index, vaccination policy, testing policy and protection of elderly respectively. In order to estimate the short-term equation, Hendry's [9] suggestion that after establishment of long-run relationship between the dependent and independent variables, the panel error correction Model (ECM) model is expressed in equation (5) as follows:

$$\Delta\text{NEW\_DEATHS}_{i,t} = \alpha_0 + \sum_{j=1}^{p} \alpha_{i,j}^{1} \Delta\text{NEW\_DEATHS}_{t-i} + \\ + \sum_{k=1}^{6} \sum_{j=0}^{qk} \alpha_{i,j}^{k+1} X_{t-j}^{k} + \Theta\text{ECM}_t - 1 + \epsilon_t, \quad (5)$$

where Θ is the ECM coefficient, which gauges the rate at which the economy adjusts each year in the direction of long-run equilibrium. The Akaike's lag selection criteria are used to establish the ECM model's ideal lag length. All the nations in the sample are considered while estimating the panel ECM.

This offers a broad overview as well as a platform of the connections between health interventions, socioeconomic observational data, and news coronavirus mortality throughout European member states. The COVID-19 death, however, is dependent on a number of factors, including the stringency index, containment health index, economic support index, vaccination policy, testing policy, and the protection of elderly people, as emphasized in the research study. Using the pooled mean group (PMG) method, the panel ARDL regression is estimated. Reference [10] describes an estimation method that combines pooling and averaging of coefficients. The intercepts, short-run coefficients, and error variances can vary freely between groups using this panel approach. The likelihood-based PMG estimator, meanwhile, imposes the restriction that the long-run coefficients be constant across groups. When homogeneity restriction is in fact true, this results in consistent estimates. The PGM estimator is also less susceptible to outliers in situations where the cross-sectional (N) is very small, as it is in our study, and it may simultaneously fix the serial autocorrelation issue. Furthermore, by selecting the proper lag structure for both the dependent and independent variables, this likelihood-based estimation resolves the issue with endogenous regressors.

3.2.4. Panel causality test

Testing for bidirectional causality between the public announcement of COVID-19's death and health treatments and socioeconomic observational data is the last step in our empirical research. Reference [11] creates a technique for analyzing the causal link between time series in a major study. The Granger representation theorem shows that there must be at least a unidirectional causality between two time series if they are cointegrated. By extending this methodology, Dumitrescu and Hurlin make it possible to identify causality in panel data. To ascertain if there is unidirectional or bidirectional causation between the two variables, the Dumitrescu and Hurlin causality test is used [12]. This two-way Granger test is used to look into the direction of causality (see equations (6), (7)):

$$\Delta\text{NEW\_DEATHS}_{i,t} = \\ = \alpha_i + \sum_{i=1}^{p} \delta_{i,k} \Delta\text{NEW\_DEATHS}_{t-k} + \sum_{k=1}^{k} \pi_{i,k} \Delta X_{t-k} + \epsilon_t, \quad (6)$$

$$\Delta X_{i,t} = \alpha_i + \sum_{i=1}^{p} \delta_{i,k} \Delta X_{t-k} + \sum_{i=1}^{p} \pi_{i,k} \Delta \text{NEW\_DEATHS}_{t-k} + \epsilon_t \quad (7)$$

with $i = 1, \ldots, N$ and $t = 1, \ldots, T$, where $X_{1,t}$ are the observations of independent variables used previously for country i in period t. In essence, equations (4) and (5) examine the significance of X's impacts on the present values of *confirmed cases* and X's effects on the present values of *confirmed cases*, respectively. Hence, the alternative is: $H_0 : \pi_{i,1} = ... = \pi_{i,k} = 0$ $\forall i = 1, \ldots, N$ which is similar to the fact that there is no proof of causality for any of the panel's countries. The possibility of causality for each of the panel's countries, but not necessarily for all of them, is another crucial premise of this test.

4. Results

4.1. Panel unit root and cointegration tests

As it's crucial to make sure that the order of integration is either zero or one for ARDL modeling, the empirical analysis should begin with the execution of the unit root test. To look for signs of stationarity, the Levin Lin Chu (LLC) first-generation unit root tests are used. Overall, the findings show that the panel's order of integration for the variables included in the analysis is $I(0)$ or $I(1)$, allowing for their use in the estimation of an ARDL model. The second stage of the study is to test for cointegration between the dependent variable and the six regressors given the strong support of Integration order in all the variables throughout our panel. The possibility that there is no cointegration in the panel is investigated using the Pedroni and Kao residual-based cointegration tests. The null hypothesis that there is no cointegration in the three panels is substantially rejected by cointegration tests. Consequently, for all three panels, there is proof of a long-term link between the dependent and explanatory factors. This implies that findings from an estimation of the Error Correction Model (ECM) will be trustworthy in both the short- and long-term.

4.2. Panel ARDL estimation

The next step is to estimate the panel ARDL regression as indicated in the ECM equation using a Pooled Mean Group (PMG) estimation. This is done after checking that the five variables are not integrated of an order equal or larger than $I(2)$ and that the series are co-integrated. Based on the AIC lag selection criterion, the appropriate lag duration is chosen.

Table 3 presents the empirical results on COVID-19 new deaths and intervention variables for the panel of 27 EU member states and for the full sample period, February 1st, 2020, to November 27, 2022.

The next step is to estimate the panel ARDL regression using a Pooled Mean Group (PMG) estimation as stated in the ECM equation. This is done after making sure the series are co-integrated and that none of the five variables are integrated to an order equal to or greater than $I(2)$. The suitable lag time is selected using the AIC lag selection criterion.

Table 3

Panel Error Correction Model estimation (Long-Run Coefficients)

Variables	Pooled Mean Estimator	
	Coefficient	Standard Error
STRINGENCY	-0.098759***	0.023735
CONTAINMENT	0.184387***	0.034941
ECONOMIC_SUP	-0.004844	0.004357
VACCINATION	-0.116884	0.075845
TESTING	-0.678345***	0.231617
PROTECTION	-0.712513***	0.200808

Note: *,**,*** indicates statistical significance at the 10%, 5%, and 1% level.

The empirical results on the relationship between public debt and economic growth are presented in the table 3 for the panel of 27 EU member states and for the entire sample period, from February 1st, 2020, to November 27th, 2022, subject to other explanatory variables. In other words, the greater the measure, the stronger the control over the spread of the virus will be since variables are highly negative. The reappearance of new deaths is not much impacted by economic assistance or immunization policies. Only containment can be thought to have a 10% chance of having a major long-term impact on news death. The responses to COVID-19 have a long-term impact on lowering the number of new diseases brought on by the pandemic.

4.3. Causality

The few empirical studies that have examined the relationship between COVID-19 new deaths, healthcare interventions, and socioeconomic observational data have produced conflicting findings. In actuality, the outcomes differ depending on the nations and epochs studied in these studies. For this reason, a panel Granger causality test is carried out in the analysis's concluding section. The Granger causality test requires that the two-time series have a long-run association, or be cointegrated, in order for it to be valid. It was established in earlier phases of the analysis that there is a long-term association between new COVID-19 fatalities and health treatments and socioeconomic observational data across all panels through panel cointegration tests. This demonstrates that the relationship between COVID-19 death and other variables must at least have a unidirectional cause (see the table 4).

The paired Dumitrescu and Hurlin Panel causality test [12] is used to determine the direction of causality. The test compares a possible alternative demonstrating causality for at least one cross-sectional unit of the panel with the null hypothesis that there is no homogenous Granger causality.

Table 5 displays the outcomes of the pairwise Dumitrescu–Hurlin panel causality tests.

Table 4

Dumitrescu and Hurlin panel causality test

Null hypothesis	W-Stat	Zbar-Stat	p-value
STRINGENCY does not Granger Cause NEW_DEATHS	18.8074	43.4847	0.0000
NEW_DEATHS does not Granger Cause STRINGENCY	1.81496	-0.48906	0.6248
CONTAINMENT does not Granger Cause NEW_DEATHS	19.0667	44.1558	0.0000
NEW_DEATHS does not Granger Cause CONTAINMENT	2.33235	0.84984	0.3954
ECONOMIC_SUP does not Granger Cause NEW_DEATHS	8.10025	15.7761	0.0000
NEW_DEATHS does not Granger Cause ECONOMIC_SUP	2.12838	0.32200	0.7475
VACCINATION does not Granger Cause NEW_DEATHS	8.48059	16.7605	0.0000
NEW_DEATHS does not Granger Cause VACCINATION	4.70284	6.98432	3.E-12
TESTING does not Granger Cause NEW_DEATHS	7.71457	14.7781	0.0000
NEW_DEATHS does not Granger Cause TESTING	1.25976	-1.92584	0.0541
PROTECT_ELD does not homogeneously cause NEW_DEATHS	7.55908	14.3758	0.0000
NEW_DEATHS does not homogeneously cause PROTECT_ELD	1.44830	-1.43794	0.1505

The results reveal that for the full group of countries, there is a bidirectional causality between new deaths and vaccination policy at a 95% confidence level. At 90% confidence level we can also consider that there is a bidirectional causality between new deaths of COVID-19 and testing policy. We can also notice that stringency, containment, economic support and help to elderly people cause new death when the contrary is not true. The sense of the causality is given in ARDL model result (coefficients of stringency and economic support to elderly are negatives meaning that more the variable increase and less will be the number of recorded cases of deaths due to COVID-19). In the other hand, more containment should lead to more deaths.

Table 5

Panel Error Correction Model estimation (Short-Run Coefficients)

Variables	Pooled Mean Estimator	
	Coefficient	Standard Error
ECT(-1)	-0.204139***	0.051513
D(NEW_DEATHS(-1))	-0.446762***	0.050073
D(NEW_DEATHS(-2))	-0.366532***	0.031000
D(NEW_DEATHS(-3))	-0.171823***	0.015298
D(CONTAINMENT)	-2.888073*	1.621810

5. Conclusion

In order to analyze the impact of health and socioeconomic interventions, we used data on European Union countries from Oxford University and WHO. We also addressed the challenges of identifying causal risk factors and evaluating the causal effects of risk factors and intervention measures on COVID-19. Overall, the pandemic preventive strategies have been successful in lowering the number of new fatalities, according to the study's findings. The Panel Autoregressive Distributed Lag (ARDL) modeling approach provided us with a way to give policy-makers some means to adopt the best containment measures in order to stop the spread and maximize the societal impact. Containment measures are the sole component that has an impact immediately. The pairwise Dumitrescu–Hurlin panel causality tests, on the other hand, show that there is a bidirectional causality between new deaths and pharmaceutical intervention factors for the entire group of countries, and that, conversely, socioeconomic intervention factors cause new deaths when the converse is not true.

References

[1] S. L. Priyadarsini and M. Suresh, "Factors influencing the epidemiological characteristics of pandemic COVID 19: a TISM approach," *International Journal of Healthcare Management*, vol. 13, no. 2, pp. 89–98, 2020. DOI: 10.1080/20479700.2020.1755804.

[2] A. Farseev, Y.-Y. Chu-Farseeva, Q. Yang, and D. B. Loo, "Understanding economic and health factors impacting the spread of covid-19 disease," *medRxiv*, 2020. DOI: 10.1101/2020.04.10.20058222. eprint: https://www.medrxiv.org/content/early/2020/06/09/2020.04.10.20058222.full.pdf.

[3] K. Tantrakarnapa, B. Bhopdhornangkul, and K. Nakhaapakorn, "Influencing factors of COVID-19 spreading: a case study of Thailand," *Journal of Public Health*, vol. 30, pp. 621–627, 2020. DOI: 10.1007/s10389-020-01329-5.

[4] W.-X. Tang, H. Li, M. Hai, and Y. Zhang, "Causal Analysis of Impact Factors of COVID-19 in China," *Procedia Computer Science*, vol. 199, no. 10229, pp. 1483–1489, 2022. DOI: 10.1016/j.procs.2022.01.189.

[5] R. Chaudhry, G. Dranitsaris, T. Mubashir, J. Bartoszko, and S. Riazi, "A country level analysis measuring the impact of government actions, country preparedness and socioeconomic factors on COVID-19 mortality and related health outcomes," *eClinical Medicine*, vol. 25, p. 100 464, 2020. DOI: 10.1016/j.eclinm.2020.100464.

[6] A. Levin, C.-F. Lin, and C.-S. J. Chu, "Unit root tests in panel data: asymptotic and finite-sample properties.," *Journal of Econometrics*, vol. 108 (1), pp. 1–24, 2002. DOI: 10.1016/S0304-4076(01)00098-7.

[7] M. H. Pesaran, T. Schuermann, and S. M. Weiner, "Modeling regional interdependencies using a global error-correcting macroeconometric model," *Journal of Business & Economic Statistics*, vol. 22, pp. 129–162, 2004. DOI: 10.1198/073500104000000019.

[8] M. Pesaran, Y. Shin, and R. J. Smith, "Bound Testing Approaches to the Analysis of Level Relationship.," *Journal of Applied Econometrics. Special Issue: In Memory of John Denis Sargan 1924–1996: Studies in Empirical Macroeconometrics*, vol. 16, no. 3, pp. 289–326, 2001. DOI: 10.1002/JAE.616.

[9] M. P. Clements and D. F. Hendry, "Forecasting in cointegrated systems," *Applied Econometrics*, vol. 10, pp. 127–146, 1995. DOI: 10.1002/jae.3950100204.

[10] S. Johansen, "Statistical analysis of cointegration vectors," *Journal of Economic Dynamics and Control*, vol. 12, no. 2–3, pp. 231–254, 1988. DOI: 10.1016/0165-1889(88)90041-3.

[11] R. Engle and C. Granger, " Cointegration and Error Correction: Representation, Estimation and Testing.," *Econometrica*, vol. 55, no. 2, pp. 251–276, 1987. DOI: 10.2307/1913236.

[12] E.-I. Dumitrescu and C. Hurlin, "Testing for Granger non-causality in heterogeneous panels," *Economic Modelling*, vol. 29, pp. 1450–1460, 2012. DOI: 10.1016/j.econmod.2012.02.014.

For citation:

K. A. Brou, Identification of COVID-19 spread factors in Europe based on causal analysis of medical interventions and socio-economic data, Discrete and Continuous Models and Applied Computational Science 31 (3) (2023) 260–272. DOI: 10.22363/2658-4670-2023-31-3-260-272.

Information about the authors:

Brou, Kouame A. — PhD student of Information Technology Department of Peoples' Friendship University of Russia named after Patrice Lumumba (RUDN University) (e-mail: broureino@gmail.com, ORCID: https://orcid.org/0000-0003-1996-577X)

УДК 519.872:519.217
PACS 07.05.Tp, 02.60.Pn, 02.70.Bf
DOI: 10.22363/2658-4670-2023-31-3-260-272
EDN: KIJKGU

Выявление факторов распространения COVID-19 в Европе на основе причинно-следственного анализа медицинских вмешательств и социально-экономических данных

К. А. Бру

Российский университет дружбы народов
ул. Миклухо-Маклая, д. 6, Москва, 117198, Россия

Аннотация. С момента появления COVID-19 было получено огромное количество данных, помогающих понять, как развивался и распространялся вирус. Анализ таких данных помогает получить новые знания, необходимые для контроля за развитием эпидемии и предоставить лицам, принимающим решения, инструменты для принятия эффективных мер по сдерживанию эпидемии и минимизации социальных последствий. Анализу влияния медицинских методов лечения и социально-экономических факторов на передачу коронавируса было уделено много внимания. В этой работе мы применяем панельное авторегрессионное моделирование с распределённым запаздыванием (ARDL) к данным Европейского союза для выявления факторов распространения COVID-19 в Европе. Наш анализ показал, что немедикаментозные меры были успешными в снижении смертности, а строгость изоляции, политика тестирования на вирус и механизмы защиты пожилых людей оказывают положительное влияние на сдерживание эпидемии. Результаты панельных тестов попарной причинно-следственной связи Думитреску–Херлина показывают, что для всех стран Евросоюза существует двунаправленная причинно-следственная связь между новыми смертями и факторами фармакологического вмешательства и что, с другой стороны, некоторые социально-экономические факторы вызывают новые смерти, когда обратное неверно.

Ключевые слова: анализ причинно-следственных связей, COVID-19, социально-экономические факторы, группа Думитреску–Херлина

Discrete & Continuous Models
& Applied Computational Science
ISSN 2658-7149 (online), 2658-4670 (print)

2023, 31 (3) 273–281
http://journals.rudn.ru/miph

Research article

UDC 519.6
PACS 07.05.Tp,
DOI: 10.22363/2658-4670-2023-31-3-273-281
EDN: KPCBBQ

Brain–computer interaction modeling based on the stable diffusion model

Eugeny Yu. Shchetinin

Financial University under the Government of the Russian Federation
49, Leningradsky Prospect, Moscow, 125993, Russian Federation

(received: August 7, 2023; revised: August 25, 2023; accepted: September 8, 2023)

Abstract. This paper investigates neurotechnologies for developing brain–computer interaction (BCI) based on the generative deep learning Stable Diffusion model. An algorithm for modeling BCI is proposed and its training and testing on artificial data is described. The results are encouraging researchers and can be used in various areas of BCI, such as distance learning, remote medicine and the creation of robotic humanoids, etc.

Key words and phrases: neural network technology, brain–computer system, stable diffusion

1. Introduction

An increasing number of researches in the field of artificial intelligence are aimed at development of neurotechnological applications using advances in generative deep learning. Many of these studies focus on using machine learning to analyze or decode brain signals, and lead to the creation of various biomedical devices that help people improve their quality of life [1]. One of the applications of machine learning in neurotechnology is modeling brain–computer interaction (BCI). There are many different approaches to BCI modeling, including the use of different machine learning models and neural network architectures. One of the recent developments in this field is Stable Diffusion (SD), which allows generating samples with a predetermined distribution using a stochastic diffusion process [2].

Stable Diffusion (Stable Diffusion) is one of the approaches for implementing stochastic diffusion, which takes into account the peculiarities of the input data distribution. In particular, Stable Diffusion is a generalized Cauchy distribution, which is a mixture of distributions with heavy tails and takes into account the presence of heavy outliers in the data. This makes Stable Diffusion particularly useful for modeling brain–computer interactions because

data from electroencephalography (EEG) or magnetoencephalography (MEG) often contain spikes and noise. Stable diffusion is the process of solving the Fokker–Planck equation, which describes the evolution of the probability density on the time axis. This probability density is usually a set of parameters or latent features that are valuable indicators for processing EEG or MEG data. Stable diffusion allows not only to generate new samples based on these parameters, but also to solve many other tasks related to data analysis, such as classification, regression, clustering, etc. [3, 4]. Moreover, it can be used in improving the quality of BCI, by improving the accuracy of decoding and computer interface control. A number of works have demonstrated the successful application of latent diffusion methods in the tasks of medical rehabilitation [5–7], research of biological structures [7, 8], development of humanoid robots [9–11].

This paper proposes a brain–computer interaction algorithm based on the Stable Diffusion model for BCI modeling in the learning process. The process of model creation is described, starting from data preparation and ending with the implementation of the model in a computer interface control application.

2. Stable Diffusion generative deep learning models

Diffusion models are machine learning models that learn to decompose random Gaussian noise step-by-step to produce a pattern of interest, such as an image [12–14]. The diffusion model has a significant disadvantage, since the denoising process is time and memory consuming. This makes the process slow and requires a lot of memory. The main reason for this is that they work in pixel space, which becomes unreasonably expensive, especially when generating high-resolution images. Stable diffusion was introduced to solve this problem because it depends on latent diffusion. Latent diffusion reduces memory and computational overhead by applying the diffusion process to a lower-dimensional latent space instead of using the actual pixel space.

Understanding the Basics of Denoising Diffusion Probabilistic Models.

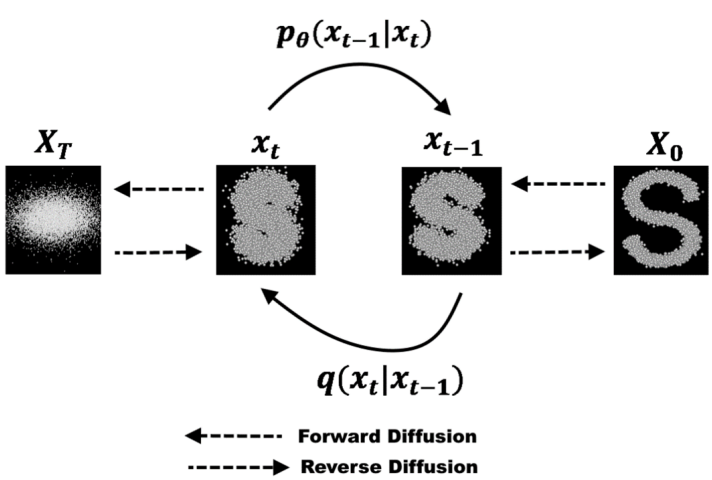

Figure 1. Process of Denoising Diffusion Probabilistic Model (Image by author)

There are three main components in latent diffusion, the most important of which is the variation autoencoder (VAE). The autoencoder (VAE) consists of two main parts: an encoder and a decoder. The encoder converts the images into a low-dimensional latent representation, which will be the input for the next component, the U-Net. The decoder does the reverse work, converting the latent representation back into an image. The U-Net is also made up of encoder and decoder parts, and both are made up of ResNet blocks. The encoder compresses the image into a lower resolution image, and the decoder decodes the lower resolution image back into a higher resolution image.

To ensure that the U-net does not lose important information when downsampling, short connections are usually added between the encoder's ResNet networks for downsampling and the decoder's ResNet networks for upsampling. In addition, a stable diffusion U-net is capable of conditioning its output to text embeddings by means of cross-attention layers. Cross-attention layers are added to both the encoding and decoding parts of the U-net, usually between ResNet blocks. The encoder is used to obtain a latent representation (latent) of the input images for the direct diffusion process during latent diffusion training. While during output, the VAE decoder converts the latent representation back into an image.

Text encoder. The text encoder converts an input query, such as "Pikachu will have a nice dinner with a view of the Eph-phil tower", into a space of embedding that can be understood by the U-net. This would be a simple transformer-based encoder that maps a sequence of tokens into a sequence of hidden embeddings of text. It is important to use a good cue to get the expected result. That's why cue engineering is trending right now. Cue engineering is the search for specific words that can make a model produce a result with certain properties.

The reason latent diffusion is fast and efficient is because the U-net of latent diffusion works in low-dimensional space. This reduces memory size and computational complexity compared to diffusion in pixel space. For example, the autoencoder used in Stable Diffusion has a reduction factor of 8. This means that the shape image (3, 512, 512) becomes (4, 64, 64) in latent space, which requires 64 times less memory. The stable diffusion model first takes a latent seed and a text cue as input. The latent seed is then used to generate random representations of latent images of size 64×64, and the text cue is converted into 77×768 text blobs using the CLIP text encoder.

The U-network then iteratively discolors the random representations of the hidden images, being conditioned by the text embeddings. The output of the U-net, which is the residual noise, is used to compute the representation of the hidden image using the scheduler algorithm. The scheduler algorithms compute the predicted representation of the cleaned image based on the previous noise representation and the predicted noise residual. Many different scheduler algorithms can be used for these calculations, each with its own pros and cons. For Stable Diffusion, we recommend using one of the following:

— PNDM scheduler (used by default);
— DDIM scheduler;
— K-LMS scheduler.

The denoising process is repeated about 50 times to get a better representation of the latent image step by step. After the process is completed, the latent image representation is decoded by a part of the variational autocoder, the decoder.

Pre-trained latent diffusion models were used to develop our project. The pre-trained diffusion model includes all the components needed to create a complete diffusion pipeline. They are stored in the following folders:

— `text_encoder`: Stable Diffusion uses CLIP, but other diffusion models may use other encoders, such as BERT.
— `tokenizer`: This must match the one used by the `text_encoder` model.
— `scheduler`: The scheduling algorithm used to postpone adding noise to the image during training.
— `U-Net`: The model used to generate a latent representation of the input data.
— `VAE`: The autoencoder module we will use to decode the latent representations into real images.

We can load the components by accessing the folder in which they were saved, using the subfolder argument for `from_pretrained` [8].

3. Developing a brain–computer interaction algorithm based on the SD model

Step 1. Data preparation

The first step in creating the Stable Diffusion model for BCI modeling is to prepare the data. As data, we will use a set of EEG data obtained from subjects who performed the task of memorizing numbers. Each experiment consisted of several trials, each of which required the subject to memorize a specific digit displayed on a screen and then reproduce it using reasoning.

EEG electrodes placed on the subjects' heads were used to acquire the data, and the signals were digitized and recorded on a computer. This data consisted of several channels and included information about the temporal distribution of the signals received from each electrode.

Before processing the data, we performed preprocessing, including noise filtering and outlier elimination. In addition, we created a function to convert the data into a format suitable for model processing and training. At this stage we have prepared the data set which contains the information about the time distribution of the EEG signals for the purpose of training and testing the Stable Diffusion model.

Step 2: Model development

After receiving the data we began to develop the model itself. In our case we chose the Stochastic Diffusion model using Stable Diffusion as the diffusion process. It is worth noting that we used the TensorFlow Probability library to implement this model [15–18]. Stable Diffusion was implemented in the form of a parametrized distribution, which is specified by two parameters – the exponent and the scale. These parameters were trained on EEG data and used to generate new samples. In addition, we used the autoencoder model to train latent features from the EEG data, which were then used as input parameters for the Stable Diffusion model. In general, the model was trained on the EEG data, which were divided into a training set, a control set, and a test set. During training, we used the maximum likelihood method

to optimize the model parameters. In addition, we used L2 regularization to prevent model overtraining.

Step 3: Testing the Model

After training the model, we proceeded to test it on the control and test datasets. We used metrics such as accuracy, AUC ROC, f1-score, and error matrix to evaluate the quality of the model. We also tested how well our model performed on new data by displaying samples created with the model and comparing them to real data. We found that our model fairly accurately reflected the distribution of the EEG data and allowed us to generate new samples that seemed similar to the real data.

Step 4: Implement the model in the application

Finally, we set about incorporating the model into a computer interface management application. We used the TensorFlow Serving library to run our model on a remote server that handled requests from the application and returned real-time predicates. In our application, the user could control the computer with his mind. He could select commands such as "up", "down", "left", and "right" just by thinking about those commands. These mental commands were passed to the TensorFlow server through our Python library, which in turn used the Stable Diffusion model to classify the user's EEG signals and determine his intentions.

Step 5: Implementing the model in the training process

After we successfully trained and tested the Stable Diffusion model for BCI modeling, we proceeded to implement it into the learning process. We created an interactive application that allows users to control the computer interface through thinking. The application is a scenario in which the user is asked to perform a task, such as moving the mouse cursor around a target and pressing buttons. To control the thinking, the user looks at a symbol that corresponds to a given command and directs his or her attention to that symbol. Then, the application's interfaces use EEG signals to recognize that symbol and execute the appropriate command.

4. Discussion of results

In this paper, we have reviewed the details of creating a Stable Diffusion model to simulate brain–computer interaction in the learning process. We described in detail how to prepare the data, develop the model, and test it to determine the quality of its performance. We also demonstrated how our Stable Diffusion model can be applied to create an interactive application that allows users to manipulate the computer interface with their thinking. The Stable Diffusion model we developed has been shown to work well in simulating brain–computer interaction in the learning process. We created a model that could process EEG data and generate new samples that matched the distribution of the real data. We also successfully incorporated this model into a computer interface control application where the user could control the

computer by thinking. Moreover, our Stable Diffusion model can solve not only the classification problem, but also some other data processing problems, such as clustering and regression. It can be used not only for modeling the interaction between the brain and the computer, but also for other tasks related to time series analysis and modeling of temporal processes. As a result, the Stable Diffusion model is a powerful tool for modeling and constructing ROC/PR curves to evaluate the quality of model performance.

To test the model we used different tasks related to EEG signal decoding. For example, we used different types of classification with a number of classes from 2 to 10, including one-vs-all and multi-class classification. We also performed clustering analysis to see which activity patterns could be extracted from the data. During model testing, we obtained high accuracy and AUC values, as well as high clustering quality. Overall, the model gave good results on all tasks, indicating its validity and applicability to BCI modeling.

One of the main advantages of modeling brain–computer interaction with Stable Diffusion is that it takes into account the peculiarities of input data distribution, which allows to work more efficiently with data containing noise and spikes. Furthermore, using Stable Diffusion maximizes the likelihood of the data, which improves the accuracy of decoding and controlling computer interfaces. Another important advantage of simulating brain–computer interaction with Stable Diffusion is that it can be run in real-time online. This is especially important when applying such a model to real-world computer interface control tasks, where fast response and accuracy are critical.

5. Conclusion

The Stable Diffusion model is a powerful tool for modeling brain–computer interaction, and can be used to create biomedical devices that help people improve their quality of life. For example, such devices can be used to control prostheses, control mouse cursors, or play computer games without using hands or voice. However, at this point, our knowledge of the actual capabilities and limits of this model and the specific solutions it can provide is far from complete, which opens up many possibilities for future research and development. The use of brain–computer interaction modeling to control computational interfaces is an experimental and promising area that has great potential for future development. However, it is also a challenging task that requires high skill and expertise in neurotechnology, machine learning, and biomedical sciences.

Successful implementation of such a model requires the use of modern data processing and analysis methods, as well as a strong technical base, including powerful computing resources and highly specialized devices for EEG and MEG data acquisition and processing.

Despite limitations and disadvantages, the use of brain–computer interaction modeling is one of the most promising and attractive directions in neurotechnology, and has the potential to significantly change our lives in the future. And in conclusion it is worth mentioning that the future of this direction is determined by how fast, scientists can develop models which can be of real interest for people and be widely used in their lives. They can change existing work processes and teach us new ways to manage the world around us through our thoughts, and help people with disabilities in their daily lives.

That is why this area is now actively researched and developed all over the world. To date, there are several successful prototypes of computer-interface control devices that use brain–computer interaction, and undoubtedly, we will see more potential applications of this technology in the future.

However, it is important to note that the use of brain–computer interaction technologies also raises ethical and safety issues. Thus, in order to achieve the most positive results, it is necessary to pay due attention to security and ethical issues, including data privacy and information security rights of individual users.

In general, the application of brain–computer interaction modeling is an important direction in neurotechnology, which opens up possibilities for a wide range of new applications. However, in order to successfully achieve the results and to use this technology in everyday life, careful work and continuous search for new solutions and improvement of technologies are needed.

References

[1] W. Li, Y. Chen, X. Huang, G. Wang, and X. Zhang, "Combining multiple statistical methods to improve EEG-based decoding for BCI applications," *Applications. IEEE Transactions on Instrumentation and Measurement*, vol. 69, no. 12, pp. 8896–8906, 2019.

[2] C. Yen and C. Lin, "A real-time brain–computer interface system for the upper limb using feedback training based on motor imagery," *IEEE Transactions on Neural Systems and Rehabilitation Engineering*, vol. 27, no. 10, pp. 2087–2096, 2019.

[3] H. Zhang, W. Zheng, K. Zhang, Y. Li, Y. Wang, and L. Yao, "Stochastic channel effects modeling and training deep spiking neural networks for brain–computer interface," *IEEE Transactions on Neural Networks and Learning Systems*, vol. 31, no. 2, pp. 350–364, 2019.

[4] D. Zhu, J. Bieger, and A. Datta, "Brain–computer interfaces in neurorehabilitation: a review of recent progress," *IEEE Transactions on Neural Systems and Rehabilitation Engineering*, vol. 27, no. 6, pp. 1319–1339, 2019.

[5] D. Wu, B. Wang, Y. Li, J. Shen, and G. Wang, "A review of EEG-based brain–computer interface for medical robotic system control," *IEEE Transactions on Neural Systems and Rehabilitation Engineering*, vol. 28, no. 6, pp. 1233–1244, 2020.

[6] S. Bhattacharya, "A brief review of brain–computer interface for neuropsychological rehabilitation," *IEEE Reviews in Biomedical Engineering*, no. 12, pp. 95–107, 2019.

[7] X. Li, D. Zhu, H. Chen, Y. Zhang, and X. Wu, "A BMI system for rehabilitation of hemiplegic patients based on transcranial direct current stimulation and affective feedback," *IEEE Transactions on Neural Systems and Rehabilitation Engineering*, vol. 27, no. 3, pp. 535–544, 2019.

[8] Z. Liu, Y. Li, L. Cheng, Q. Zhang, M. Wang, L. Kong, and Y. Wang, "An EEG-based brain–computer interface system for independent living of people with cerebral palsy," *IEEE Journal of Biomedical and Health Informatics*, vol. 24, no. 7, pp. 1927–1935, 2020.

[9] Y. Hu, Y. Hou, M. Wang, T. Yu, and J. Zhang, "EEG-based motor imagery BCI system via supervised joint blind source separation and convolutional neural network," *IEEE Transactions on Neural Systems and Rehabilitation Engineering*, no. 29, pp. 1586–1597, 2021.

[10] G. Choi, W. Ko, Y. Jung, S. Jo, K. Kim, and S. Lee, "A review on recent progress in EEG-based brain–computer interface for assistive robotic control," *IEEE Reviews in Biomedical Engineering*, no. 12, pp. 141–157, 2019.

[11] M. Rashid, J. Höhne, G. Schmitz, and G. Müller-Putz, "A review of humanoid robots controlled by brain–computer interfaces," *Frontiers in Neurorobotics*, no. 14, pp. 1–28, 2020.

[12] J. Ho, A. Jain, and P. Abbeel, *Denoising diffusion probabilistic models*, 2020. DOI: 10.48550/arXiv.2006.11239.

[13] P. Dhariwal and A. Nichol, *Diffusion models beat GANs on image synthesis*, 2021. DOI: 10.48550/arXiv.2105.05233.

[14] R. Rombach, A. Blattmann, D. Lorenz, P. Esser, and O. B., *High-resolution image synthesis with latent diffusion models*, 2021. DOI: 10.48550/arXiv.2112.10752.

[15] A. Blattmann, R. Rombach, K. Oktay, and B. Ommer. "Latent diffusion models." (2022), [Online]. Available: https://github.com/CompVis/latent-diffusion.

[16] J. Sohl-Dickstein, E. A. Weiss, N. Maheswaranathan, and S. Ganguli, *Deep unsupervised learning using nonequilibrium thermodynamics*, 2015. DOI: 10.48550/arXiv.1503.03585.

[17] M. Welling and Y. W. Teh, "Bayesian learning via stochastic gradient Langevin dynamics," in *Proceedings of the 28th International Conference on International Conference on Machine Learning*, ser. ICML'11, Madison, WI, USA: Omnipress, 2011, pp. 681–688. DOI: 10.5555/3104482.3104568.

[18] J. Ho, A. Jain, and P. Abbeel, *Denoising diffusion probabilistic models*, 2020. DOI: 10.48550/arXiv.2006.11239.

For citation:

E. Y. Shchetinin, Brain–computer interaction modeling based on the stable diffusion model, Discrete and Continuous Models and Applied Computational Science 31 (3) (2023) 273–281. DOI: 10.22363/2658-4670-2023-31-3-273-281.

Information about the authors:

Shchetinin, Eugeny Yu. — Doctor of Physical and Mathematical Sciences, Lecturer of Department of Mathematics, Financial University under the Government of the Russian Federation (e-mail: riviera-molto@mail.ru, ORCID: https://orcid.org/0000-0003-3651-7629)

УДК 519.6
PACS 07.05.Tp,
DOI: 10.22363/2658-4670-2023-31-3-273-281
EDN: KPCBBQ

Моделирование взаимодействия «мозг – компьютер» на основе модели стабильной диффузии

Е. Ю. Щетинин

Финансовый университет при Правительстве Российской Федерации
Ленинградский проспект, д. 49, Москва, 125993, Россия

Аннотация. В этой статье исследуются нейротехнологии для развития взаимодействия «мозг – компьютер» (BCI) на основе генеративной модели стабильной диффузии с глубоким обучением. Предложен алгоритм моделирования BCI и описано его обучение и тестирование на искусственных данных. Полученные результаты обнадёживают исследователей и могут быть использованы в различных областях BCI, таких как дистанционное обучение, удалённая медицина, создание роботов-гуманоидов и т. д.

Ключевые слова: технология нейронных сетей, система мозг-компьютер, стабильная диффузия